Table 1 Patients' profiles in this study: five original and an additional four reported patients

Clinical features	Original patients					Previously reported patients			
	Patient 1	Patient 2	Patient 3	Patient 4	Patient 5	Patient A[2]	Patient B[3]	Patient C[4]	Patient D[5]
Age at onset, y/sex	81/F	74/M	78/M	58/M	72/M	77/F	65/F	70/F	80/M
Duration until appearance of each clinical symptom, mo									
Myoclonic jerk	−*	5	8	10	4	6	14	9	+†
Visual or cerebellar symptom	−*	−‡	−‡	−§	−‡	−‡	−‡	−‡	−‡
Akinetic mutism	−*	12	18	−§	10	18	14	9	>18
Higher cortical dysfunction‖	−	−	+	+	+	−	+	+	+
Parkinsonism‖	−	−	+	−	−	+	−	−	−
NSE value in CSF, ng/mL	32.1	13.0	19.5	22.0	60.4	NE	NE	NE	29.9
14-3-3 protein in CSF	+	−	+	−	NE	NE	NE	NE	NE
Duration from onset to CSF study, mo	3	6	1	4	3	5	Uncertain	2	1
PSWC in EEG	−	−	−	−	−	−	−	−	−
Codon 129 in *PRNP*	M/V	M/M	M/V	M/V	M/M	M/V	M/M	M/M	M/V
PrP staining	NE	NE	NE	NE	NE	+	NE	+	±

Patient A was previously reported by Matsumura et al.[2] Patient B was previously reported by Ishida et al.[3] Patient C was previously reported by Kobayashi et al.[4] Patient D was previously reported by Iwasaki et al.[5]

* We could not detect referring symptoms during our observation period in Patient 1 (until 15 mo after the onset). † The duration until the appearance of myoclonic jerk in Patient D is uncertain. ‡ We or the authors could not detect visual or cerebellar symptoms during the observation period. The patients' severe dementia or consciousness disturbance prevented us from making a close neurologic examination in the advanced stage.
§ We could not detect the referring symptoms during our observation period in Patient 4 (until 16 mo after the onset).
‖ The presence or lack of presence as initial symptoms.

NSE = neuron-specific enolase; NE = not examined; PSWC = periodic sharp and wave complexes; *PRNP* = prion protein gene; M/V = methionine/valine heterozygosity at codon 129 in *PRNP*; M/M = methionine homozygosity at codon 129 in *PRNP*; PrP = prion protein.

Table 2 Comparison of clinical features between CJD180 and sCJD

Features	CJD with MM129			CJD with MV129		
	CJD180	sCJD	*p* value	CJD180	sCJD	*p* value
Age at onset, y	70.3 ± 3.9 (n = 4)	65.3 ± 11.6 (n = 116)	0.32	74.8 ± 9.5 (n = 5)	62.6 ± 10.5 (n = 5)	<0.05
Myoclonic jerk, mo*†	8.0 ± 4.5 (n = 4)	2.7 ± 2.4 (n = 113)	<0.01	9.8 ± 3.9 (n = 4)	8.2 ± 5.1 (n = 5)	0.71
Akinetic mutism, mo*‡	11.3 ± 2.2 (n = 4)	3.5 ± 2.8 (n = 113)	<0.005	17.0 ± 1.4 (n = 5)	10.4 ± 5.4 (n = 5)	<0.05
Visual symptom, %§	0.0 (n = 4)	24.0 (n = 96)	0.26	0.0 (n = 5)	20.0 (n = 5)	0.29
Cerebellar symptom, %§	0.0 (n = 4)	12.5 (n = 96)	0.45	0.0 (n = 5)	40.0 (n = 5)	0.11
Higher cortical dysfunction, %§	75.0 (n = 4)	5.2 (n = 96)	<0.0001	60.0 (n = 5)	0.0 (n = 5)	<0.05
NSE value, ng/mL‖	36.7 ± 33.5 (n = 2)	75.9 ± 65.7 (n = 66)		25.9 ± 6.1 (n = 4)	50.6 ± 7.9 (n = 2)	
Positive rate of NSE, %‖¶	50.0 (n = 2)	72.7 (n = 66)		0.0 (n = 4)	100.0 (n = 2)	
Positive rate of 14-3-3 protein, %‖	0.0 (n = 1)	87.7 (n = 65)		66.7 (n = 3)	100.0 (n = 2)	
PSWC in EEG, %	0.0 (n = 4)	94.0 (n = 116)	<0.0001	0.0 (n = 5)	60.0 (n = 5)	<0.05

Values are means ± SD where applicable.

* The duration until the appearance of referring symptoms.
† Patient 1 had not demonstrated myoclonic jerk 15 mo after the onset, and we accepted 15 mo for the statistical comparison. Patient D[5] demonstrated myoclonic jerk, but we could not identify the duration until the appearance. Therefore, we eliminated Patient D from the statistical comparison.
‡ Patients 1 and 4 had not become akinetic and mute, and we could not identify the date when Patient D[5] become akinetic and mute. Therefore, for the statistical comparison, we accepted the date when they were last confirmed not to be akinetic and mute, i.e., 15 mo for Patient 1, 16 mo for Patient 4, and 18 mo for Patient D.
§ The rate of referring symptoms as initial symptoms.
‖ NSE or 14-3-3 protein in CSF.
¶ The cut-off value was 35.0 ng/mL.

CJD = Creutzfeldt–Jakob disease; sCJD = sporadic CJD; NSE = neuron-specific enolase; PSWC = periodic sharp and wave complex.

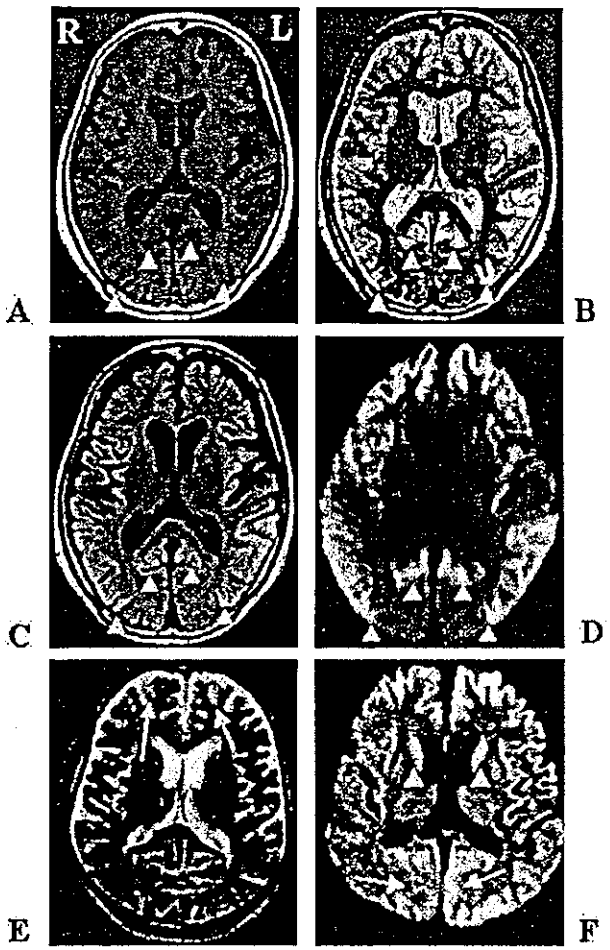

Figure. MRI of Patient 1 (A through D) and a patient with sporadic Creutzfeldt–Jakob disease (CJD) (E and F). For Patient 1 (82-year-old woman), the MRI studies were performed 4 months after the onset using 1.5 T MR unit (Magnetom Vision; Siemens, Erlangen, Germany) equipped with a conventional head coil. At this time, she demonstrated only memory disturbance and could perform her daily activities with minimal support. The wide-ranging cortical ribbon is symmetrically depicted as a low-intensity lesion by T1-weighted imaging (A) and as a high-intensity lesion by T2-weighted (B), fluid-attenuated inversion recovery (C), and diffusion-weighted (D) imaging and has a swollen appearance. The basal ganglia are not involved. Characteristically, the medial regions posterior to the parieto-occipital sulcus in the occipital lobes are not involved (arrowheads). The cerebellum was not depicted as an abnormal-intensity lesion (data not shown). For the patient with sporadic CJD with methionine homozygosity at codon 129 (70-year-old man), the MRI studies were performed 2 months after the onset using the same MR unit. At this time, he was totally bedridden and did not respond to any simple orders but opened his eyes when his name was called loudly. He showed myoclonus and startle reflex. The wide-ranging cortical ribbon including the occipital lobe (arrows) and the bilateral caudate heads (arrowheads) are depicted as a high-intensity lesion by diffusion-weighted imaging (F), although T2-weighted imaging examined at the same time demonstrates a high-intensity lesion in only the frontal lobe (arrows).

were recognized in three of four CJD180 cases with MM129 and three of five CJD180 cases with MV129 in the very early phase. On the other hand, no CJD180 patients demonstrated visual or cerebellar symptoms, which were cardinal in sCJD. Irrespective of the polymorphism at codon 129, no CJD180 patients demonstrated PSWC in repeated EEG in their disease course.

In the MRI study, the wide range of the cortical ribbon was depicted as a low-intensity area by T1I and a high-intensity area by T2I, FLAIR, and DWI and had a swollen appearance (figure, A through D). These cortical lesions were remarkable compared with the severity of the clinical symptoms. The basal ganglia lesions were less remarkable compared with the cortical lesions. Characteristically, the medial regions, posterior to the parieto-occipital sulcus in the occipital lobes (see the figure, A through D, arrowheads), and the cerebellum were never involved in the early stage. These cortical lesions were not always symmetric in the first MRI. In sequential MRI performed in six of seven patients, these cortical lesions expanded and, in one patient,[9] finally included the medial occipital regions. The swollen cortical lesions became atrophied in the advanced stage, but not as severe as compared with the brain atrophy of sCJD.

Discussion. V180I is recognized as a causative point mutation based on the result that V180I was detected only in CJD patients but not in 200 normal Japanese persons.[9] The World Health Organization also lists CJD180 as familial CJD.[1]

We clarified the clinical and laboratory characteristics of CJD180 by comparing them with those of sCJD. CJD180 showed 1) older onset age; 2) slower progression of the disease; 3) unique clinical symptoms such as frequent higher cortical dysfunction, which was less frequent in sCJD, no visual or cerebellar symptoms, which were important for sCJD, and less remarkable myoclonic jerk compared with the generalized one in sCJD; 4) a lower positive rate of brain-specific proteins such as NSE and 14-3-3 protein in CSF; and 5) no PSWC in EEG throughout the disease course. These features render it difficult to make a premortem diagnosis of CJD180 based on the clinical features without a *PRNP* analysis.

In our experience, the most useful test leading to the genetic analysis was MRI. The abnormal lesions in MRI of sCJD are varied,[10] but those of CJD180 are rather uniform. In accordance with the absence of visual or cerebellar symptoms in the early stage, the medial occipital lobes posterior to the parieto-occipital sulcus or the cerebellum were never involved until the terminal stage. A disproportionately remarkable cortical lesion compared with the severity of the clinical symptoms and less remarkable basal ganglia lesion must be recognized as characteristic MRI findings. At present, we must recognize an uncommon variant of familial CJD that might have been misdiagnosed. Therefore, we recommend MRI study including DWI for patients with progressive dementia. Then, we should perform a *PRNP* analysis

in all patients with progressive dementia and characteristic MRI abnormalities.

Parkinsonism, which was a rare symptom in sCJD, occurred in two of five CJD180 cases with MV129 in the very early stage. It is important to discriminate among neurodegenerative disorders presenting dementia with parkinsonism from CJD180. MRI can provide us useful information.

CJD180 is clearly associated with a point mutation of *PRNP* but appears as if it were a sporadic neurodegenerative disorder. We may misdiagnose such cases without a genetic analysis because of the difference in the clinical features from what we usually consider the "CJD characteristic" clinical features. Characteristic MRI findings can lead us to an accurate premortem diagnosis.

Acknowledgment

The authors thank Drs. Nobuhito Seno, Takafumi Hasegawa, Michiko Matsuzaki, Masahiro Asano, Atsushi Takeda, and Nobuyuki Sato for clinical support; Drs. Shuichi Higano and Shoki Takahashi for performing the MRI study; and Mr. Brent Bell for reading the manuscript.

References

1. Zeidler M, Gibbs CJJr, Meslin F. WHO manual for strengthening diagnosis and surveillance of Creutzfeldt-Jakob disease. Geneva: World Health Organization, 1998.
2. Matsumura T, Kojima S, Kuroiwa Y, et al. An autopsy-verified case of Creutzfeldt–Jakob disease with codon 129 polymorphism and codon 180 point mutation. Clin Neurol 1995;35:282–285.
3. Ishida S, Sugino M, Koizumi N, et al. Serial MRI in early Creutzfeldt–Jakob disease with a point mutation of prion protein at codon 180. Neuroradiology 1995;37:531–534.
4. Kobayashi S, Ohuchi T, Maki T, et al. A case of probable Creutzfeldt–Jakob disease with a point mutation of prion protein gene codon 180 and atypical MRI findings. Clin Neurol 1997;37:671–674.
5. Iwasaki Y, Sone M, Kato T, et al. Clinicopathological characteristics of Creutzfeldt–Jakob disease with a PrP V180I mutation and M129V polymorphism on different alleles. Clin Neurol 1999;39:800–806.
6. Hitoshi S, Nagura H, Yamanouchi H, et al. Double mutations at codon 180 and codon 232 of the PRNP gene in an apparently sporadic case of Creutzfeldt–Jakob disease. J Neurol Sci 1993;120:208–212.
7. Nakamura Y, Watanabe M, Sato T, et al. Results of Creutzfeldt–Jakob disease surveillance in Japan. In: Hizusawa H, ed. Annual report of the Prion Disease and Slow Virus Infection Research Committee, The Ministry of Health, Labour and Welfare. 2003:26–29.
8. Aksamit AJJr, Preissner CM, Homburger HA. Quantitation of 14-3-3 and neuron-specific enolase proteins in CSF in Creutzfeldt–Jakob disease. Neurology 2001;57:728–730.
9. Kitamoto T, Ohta M, Doh-ura K, et al. Novel missense variants of prion protein in Creutzfeldt–Jakob disease or Gerstmann–Sträussler syndrome. Biochem Biophys Res Commun 1993;191:709–714.
10. Murata T, Shiga Y, Higano S, et al. Conspicuity and evolution of lesions in Creutzfeldt–Jakob disease at diffusion-weights imaging. AJNR Am J Neuroradiol 2002;23:1164–1172.

Heidenhain Variant of Creutzfeldt-Jakob Disease: Diffusion-Weighted MRI and PET Characteristics

Yoshihisa Tsuji, MD
Hiroshi Kanamori, MD
Gaku Murakami, MD
Masayuki Yokode, MD
Takahiro Mezaki, MD
Katsumi Doh-ura, MD
Ken Taniguchi, MD
Kozo Matsubayashi, MD
Hidenao Fukuyama, MD
Toru Kita, MD
Makoto Tanaka, MD

ABSTRACT

Creutzfeldt-Jakob disease (CJD) is characterized by rapidly progressive dementia with a variety of neurological disorders and a fatal outcome. The authors present a case with visual disturbance as a leading symptom and rapid deterioration in global cognitive functions. The cerebrospinal fluid was positive for 14-3-3 protein, and diffusion-weighted magnetic resonance imaging (MRI) showed marked hyperintensity in the parieto-occipital cortices, where hypometabolism was clearly detected on positron emission tomography (PET). Pattern-reversal visual evoked potentials showed prolonged P100 latencies and increased N75/P100 amplitudes. All these findings supported a diagnosis of the Heidenhain variant of CJD, whereas a long clinical course, a lack of myoclonus, and an absence of periodic synchronous discharges on electroencephalography were atypical. Diffusion-weighted MRI and PET in combination with visual evoked potential recording and 14-3-3 protein detection may be useful for the early diagnosis of CJD.

Key words: Creutzfeldt-Jakob disease, visual disturbance, 14-3-3 protein, diffusion-weighted MRI, PET, visual evoked potentials.

Tsuji Y, Kanamori H, Murakami G, Yokode MD, Mezaki T, Doh-ura K, Taniguchi K, Matsubayashi K, Fukuyama H, Kita T, Makoto T. Heidenhain variant of Creutzfeldt-Jakob disease: diffusion-weighted MRI and PET characteristics. J Neuroimaging 2004;14:63-66.
DOI: 10.1177/1051228403258147

Creutzfeldt-Jakob disease (CJD) is a rare spongiform encephalopathy occurring sporadically in most cases. The diagnosis of CJD is based on clinical symptoms, such as rapidly progressive dementia, myoclonus, visual or cerebellar signs, pyramidal or extrapyramidal signs, and akinetic mutism, although the definite diagnosis of CJD requires pathological findings of the brain.[1] Periodic synchronous discharges (PSDs) on electroencephalography (EEG) and the detection of 14-3-3 protein in the cerebrospinal fluid (CSF) further support clinical suspicion of CJD.[1-4] Furthermore, magnetic resonance imaging (MRI), particularly diffusion-weighted imaging (DWI), has been shown to be useful in diagnosing the disease.[5-12] Herein, we report a probable case of CJD in which neuroimaging techniques proved useful in the early diagnosis of the disease. Progressive dementia, visual disturbance, 14-3-3 protein in the CSF, and neuroimaging findings supported a diagnosis of CJD, but other clinical manifestations were atypical, including a long clinical course, the absence of myoclonus, and no PSDs on EEG.

Case Presentation

A 54-year-old woman noticed blurred vision and visual metamorphosis in August 2001. Her visual disturbance worsened, and she gave up driving a car. At 2 months, her family noticed that she had memory impairment and disorientation for time and place. She often lost her way around her house. Her cognitive deterioration rapidly progressed, and she felt difficulties in

Received March 31, 2003, and in revised form May 6, 2003. Accepted for publication May 9, 2003.

From the Departments of Geriatric Medicine (YT, HK, GM, MT), Neurology (TM), Functional Brain Imaging, Human Brain Research Center (HF), and Cardiovascular Medicine (TK), Graduate School of Medicine, Kyoto University, Kyoto, Japan; the Translational Research Center, Faculty of Medicine, Kyoto University (MY); the Department of Neuropathology, Neurological Institute, Kyushu University, Kyushu, Japan (KD); the Department of Psychiatry, Shoraiso National Hospital (KT); and the Center for Southeast Asian Studies, Kyoto University (KM).

Address correspondence to Makoto Tanaka, MD, Department of Geriatric Medicine, Graduate School of Medicine, Kyoto University, 54 Shogoin-Kawahara-cho, Sakyo-ku, Kyoto 606-8507, Japan. E-mail: makoto@kuhp.kyoto-u.ac.jp.

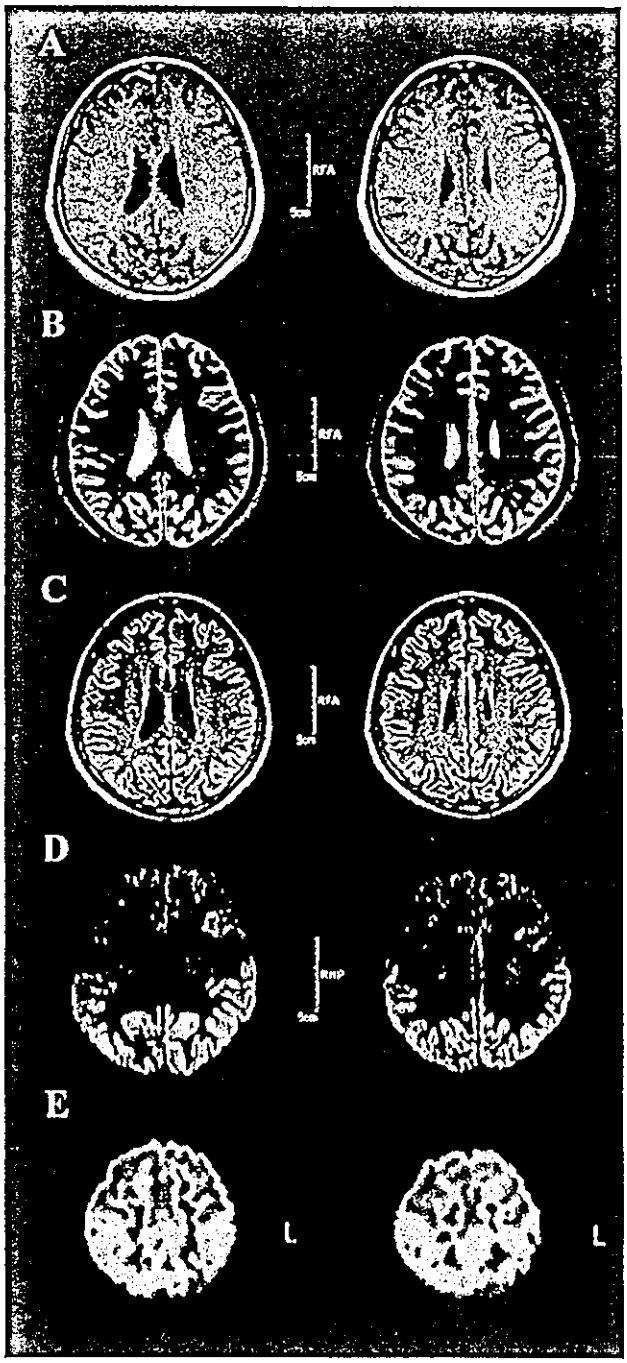

Fig 1. Magnetic resonance imaging (MRI) and positron emission tomography (PET) axial images. There was no atrophy, signs of cerebrovascular disease, or obvious signal abnormality on T1-weighted or T2-weighted MRI (A, B). High signal intensity in the parieto-occipital regions was detected on fluid-attenuated inversion recovery MRI (C), and the hyperintensity was most obvious on diffusion-weighted MRI (D). Low glucose metabolism was observed in the parieto-occipital regions as well as in the posterior cingulate cortex on PET (E). For the PET study, 5 mCi of [^{18}F]-fluorodeoxyglucose were administered intravenously, and scanning was performed using GE Advance (GE Medical Systems, Milwaukee, WI). Semiquantitative measurements were used.

calculation, reading, writing, and cooking at the beginning of 2002. She was often unable to locate the bathroom in her house by March 2002.

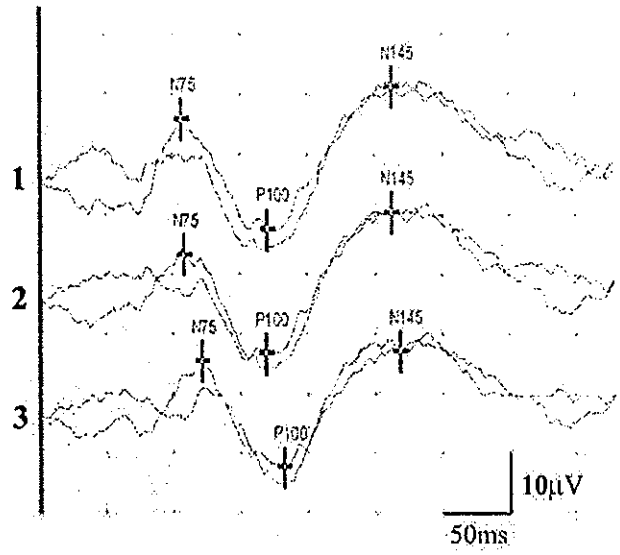

	Latency (ms)	Latency (ms)	Latency (ms)		Amplitude (μV)	Amplitude (μV)
1	N75 106	P100 170	N145 262		N75P100 18.75	P100N145 24.11
2	N75 108	P100 169	N145 262		N75P100 17.03	P100N145 24.27
3	N75 121	P100 182	N145 268		N75P100 18.38	P100N145 20.16

Fig 2. Pattern-reversal visual evoked potentials (VEPs). Binocular full-field pattern-reversal VEPs revealed prolonged P100 latencies and increased N75/P100 amplitudes. The active electrodes were placed on the left (1), the median (2), and the right (3) occipital scalp.

When she was admitted to Kyoto University Hospital in April 2002, she complained only of visual disturbance. Her medical history included operations for appendicitis and uterocervical cancer. There was no family history of dementia or psychiatric disease. She was not taking any regular medications. A neurological examination disclosed memory impairment, disorientation, anomia, alexia, agraphia, acalculia, dressing apraxia, color agnosia, and visual metamorphosis. A cranial nerve examination was normal. There were no pyramidal, extrapyramidal, or cerebellar signs or involuntary movements, including myoclonus. Her score on the Mini-Mental State Examination was 12 of 30, and she obtained a total IQ score of 48 on the Wechsler Adult Intelligence Scale–Revised.

The results of a blood test and a CSF examination were unremarkable except for positive 14-3-3 protein in the CSF. Lactic or pyruvic acid was not elevated in the CSF, and paraneoplastic markers, including anti-Hu and anti-Yo, were not detectable either in serum or in the CSF. Notably, an MRI examination revealed symmetric, bilateral, cortical hyperintensity in the parieto-occipital regions (Figs 1C, 1D). DWI most strikingly showed abnormalities in these areas (Fig 1D). There was no mass effect, atrophy, or signs of cerebrovascular disease (Figs 1A–1D). Moreover, positron emission tomography (PET) demonstrated metabolic disturbance in the parietal, occipital, and posterior cingulate cortices (Fig 1E). EEG showed diffuse slowing without typical PSDs. Pattern-reversal visual evoked potentials (VEPs) showed prolonged P100 latencies and increased N75/P100 amplitudes (normal P100 latency < 132 milliseconds,

normal N75/P100 amplitude < 10 μV[13]) (Fig 2). Genetic studies on the prion protein gene (PRNP) demonstrated no known mutations but disclosed homozygosity for methionine at the polymorphic codon 129. A brain biopsy could not be performed because we could not obtain permission from the patient's family.

At 16 months after the initial symptoms, limb and neck rigidity became apparent. At 20 months, she cannot recognize even her family members and has difficulty in oral communication because of the progression of agnosia and aphasia.

Discussion

Visual disturbance as a leading symptom, rapidly progressive dementia, and the detection of 14-3-3 protein in the CSF suggested a diagnosis of the Heidenhain variant of CJD.[14] Methionine homozygosity at codon 129 of the PRNP gene was consistent with this subtype.[15] However, this case did not fulfill the criteria for even possible CJD until the patient exhibited pronounced rigidity at 16 months after the initial symptoms.[1] This was due to the lack of some common clinical manifestations of CJD in this patient, including myoclonus, ataxia, and PSDs on EEG. This case not only suggests a heterogeneity of clinical presentation among patients with CJD but indicates difficulty in the early diagnosis of CJD without typical presentation. Currently used diagnostic criteria based on clinical symptoms and EEG findings may miss some CJD cases without typical sets of clinical manifestations, as in this case. Therefore, it is important to use neuroimaging and laboratory examinations for the early diagnosis of the disease.

Increased T2-weighted MRI signal has been described in the basal ganglia,[5,8] and recently, cortical hyperintensity was shown on diffusion-weighted MRI in some CJD cases with typical clinical courses.[6,7,10,11,16] Moreover, areas of signal abnormalities on diffusion-weighted MRI were well correlated with the neuropathologic findings of spongiform encephalopathy.[10] In the present case, hyperintensity in the parieto-occipital lobes was clearly shown on diffusion-weighted MRI early in the clinical course, indicating that diffusion-weighted MRI is useful for the early diagnosis of CJD.

There has been a relatively limited number of reports describing PET studies of CJD.[6,17,18] Henkel et al[18] analyzed PET studies of 8 patients with CJD and found decreased glucose metabolism in the occipital lobe, cerebellum, or basal ganglia in addition to temporal or parietal cortical region. In the preset case, metabolic disturbance was observed in the parietal, occipital, and posterior cingulate cortices. Although metabolic reductions in the parietal and posterior cingulate cortices are seen in other dementing diseases,[19,20] the clear involvement of the occipital lobes differed from the typical pattern of disturbance detected in Alzheimer's disease,[20] which is the most frequent misdiagnosis of CJD.[21] It may be more difficult to distinguish dementia with Lewy bodies (DLB) from CJD on PET, because significant metabolic reductions in the occipital cortex can be also seen in DLB.[20,22] Diffusion-weighted MRI and 14-3-3 protein detection may be useful in the differential diagnosis of the 2 diseases.[23]

VEPs may also provide a diagnostic aid for the early detection of CJD. According to previous reports, P100 latencies were increased or normal, but increased P100 amplitudes were the most frequent finding in CJD patients, particularly during the early stages of the disease.[13,24,25] Our case also showed increased P100 amplitudes at the early phase of the disease, thus indicating that VEP recording may be helpful, particularly in the early diagnosis of CJD without typical clinical presentation.

14-3-3 protein is expressed in all eukaryotic cells and participates in the regulation of diverse biological processes, including neuronal development, cell growth control, and cell cycling. There are 7 isoforms, 5 of which are present in neuronal cells and constitute nearly 1% of all soluble brain proteins.[26] The detection of 14-3-3 protein in the CSF probably reflects severe neuronal destruction.[23] 14-3-3 protein in the CSF has been shown to be a useful biochemical marker for CJD,[2,4] and Zerr et al[4] demonstrated that the specificity was even higher than that of PSDs on EEG. In the recent revised version of the French and European study criteria, positive 14-3-3 protein detection is considered as a criterion equivalent to a typical EEG.[1] According to the revised version, our patient was classified as probable CJD.

CJD may be a more heterogeneous group of disorders than has been recognized, and neuroimaging techniques, including diffusion-weighted MRI and PET, in combination with VEPs and 14-3-3 protein detection may be useful for the early diagnosis of CJD.

References

1. Brandel JP, Delasnerie-Laupretre N, Laplanche JL, Hauw JJ, Alperovitch A. Diagnosis of Creutzfeldt-Jakob disease: effect of clinical criteria on incidence estimates. *Neurology* 2000;54:1095-1099.
2. Hsich G, Kenney K, Gibbs CJ, Lee KH, Harrington MG. The 14-3-3 brain protein in cerebrospinal fluid as a marker for transmissible spongiform encephalopathies. *N Engl J Med* 1996;335:924-930.
3. Staffen W, Trinka E, Iglseder B, Pilz P, Homann N, Ladurner G. Clinical and diagnostic findings in a patient with Creutzfeldt-Jakob disease (type Heidenhain). *J Neuroimaging* 1997;7:50-54.
4. Zerr I, Pocchiari M, Collins S, et al. Analysis of EEG and CSF 14-3-3 proteins as aids to the diagnosis of Creutzfeldt-Jakob disease. *Neurology* 2000;55:811-815.
5. Finkenstaedt M, Szudra A, Zerr I, et al. MR imaging of Creutzfeldt-Jakob disease. *Radiology* 1996;199:793-798.
6. Na DL, Suh CK, Choi SH, et al. Diffusion-weighted magnetic resonance imaging in probable Creutzfeldt-Jakob disease: a clinical-anatomic correlation. *Arch Neurol* 1999; 56:951-957.
7. Demaerel P, Heiner L, Robberecht W, Sciot R, Wilms G. Diffusion-weighted MRI in sporadic Creutzfeldt-Jakob disease. *Neurology* 1999;52:205-208.
8. Schroter A, Zerr I, Henkel K, Tschampa HJ, Finkenstaedt M, Poser S. Magnetic resonance imaging in the clinical diagnosis of Creutzfeldt-Jakob disease. *Arch Neurol* 2000;57: 1751-1757.
9. Jacobs DA, Lesser RL, Mourelatos Z, Galetta SL, Balcer LJ. The Heidenhain variant of Creutzfeldt-Jakob disease: clinical, pathologic, and neuroimaging findings. *J Neuroophthalmol* 2001;21:99-102.
10. Mittal S, Farmer P, Kalina P, Kingsley PB, Halperin J. Correlation of diffusion-weighted magnetic resonance imaging with neuropathology in Creutzfeldt-Jakob disease. *Arch Neurol* 2002;59:128-134.

11. Rabinstein AA, Whiteman ML, Shebert RT. Abnormal diffusion-weighted magnetic resonance imaging in Creutzfeldt-Jakob disease following corneal transplantations. *Arch Neurol* 2002;59:637-639.
12. Eschweiler GW, Wormstall H, Widmann U, Naegele T, Bartels M. Correlation of diffusion-weighted magnetic resonance imaging with neurological deficits in sporadic Creutzfeldt-Jakob Disease. *Nervenarzt* 2002;73:883-886.
13. de Seze J, Hache JC, Vermersch P, et al. Creutzfeldt-Jakob disease: neurophysiologic visual impairments. *Neurology* 1998;51:962-967.
14. Kropp S, Schulz-Schaeffer WJ, Finkenstaedt M, et al. The Heidenhain variant of Creutzfeldt-Jakob disease. *Arch Neurol* 1999;56:55-61.
15. Parchi P, Giese A, Capellari S, et al. Classification of sporadic Creutzfeldt-Jakob disease based on molecular and phenotypic analysis of 300 subjects. *Ann Neurol* 1999;46: 224-233.
16. Bahn MM, Parchi P. Abnormal diffusion-weighted magnetic resonance images in Creutzfeldt-Jakob disease. *Arch Neurol* 1999;56:577-583.
17. Grunwald F, Pohl C, Bender H, et al. 18F-fluorodeoxyglucose-PET and 99mTc-bicisate-SPECT in Creutzfeldt-Jakob disease. *Ann Nucl Med* 1996;10:131-134.
18. Henkel K, Zerr I, Hertel A, et al. Positron emission tomography with [(18)F]FDG in the diagnosis of Creutzfeldt-Jakob disease (CJD). *J Neurol* 2002;249:699-705.
19. Minoshima S, Giordani B, Berent S, Frey KA, Foster NL, Kuhl DE. Metabolic reduction in the posterior cingulate cortex in very early Alzheimer's disease. *Ann Neurol* 1997; 42:85-94.
20. Minoshima S, Foster NL, Sima AA, Frey KA, Albin RL, Kuhl DE. Alzheimer's disease versus dementia with Lewy bodies: cerebral metabolic distinction with autopsy confirmation. *Ann Neurol* 2001;50:358-365.
21. Poser S, Mollenhauer B, Kraubeta A, et al. How to improve the clinical diagnosis of Creutzfeldt-Jakob disease. *Brain* 1999;122:2345-2351.
22. Lobotesis K, Fenwick JD, Phipps A, et al. Occipital hypoperfusion on SPECT in dementia with Lewy bodies but not AD. *Neurology* 2001;56:643-649.
23. Haik S, Brandel JP, Sazdovitch V, et al. Dementia with Lewy bodies in a neuropathologic series of suspected Creutzfeldt-Jakob disease. *Neurology* 2000;55:1401-1404.
24. Aguglia U, Farnarier G, Regis H, Oliveri RL, Quattrone A. Sensory evoked potentials in Creutzfeldt-Jakob disease. *Eur Neurol* 1990;30:157-161.
25. Finsterer J, Bancher C, Mamoli B. Giant visually-evoked potentials without myoclonus in the Heidenhain type of Creutzfeld-Jakob disease. *J Neurol Sci* 1999;167:73-75.
26. Green AJ. Use of 14-3-3 in the diagnosis of Creutzfeldt-Jakob disease. *Biochem Soc Trans* 2002;30:382-386.

＜シンポジウム 8—4＞神経感染症の克服をめざして

プリオン病：遺伝子異常と臨床像・病理像および治療薬開発の展望

堂浦　克美

（臨床神経，44：855—856，2004）
Key words：変異型クロイツフェルト・ヤコブ病，鑑別診断，治療，抗マラリア薬，ペントサンポリサルフェート

はじめに

ウシ海綿状脳症の発生が欧州・アジア・北米に拡大し，変異型CJDがわが国で発生しても不思議ではない状況にある．一方，わが国では多数の硬膜移植後のCJDが発生しており，これらの後天性プリオン病は，他の神経精神疾患だけでなく遺伝性プリオン病や孤発性プリオン病との鑑別も必要である．今回，とくに若年者での発生が危惧されている変異型CJDの診断について，鑑別を要する非定型的プリオン病ついて概説する．また，これらの後天性プリオン病の発生を背景として，最近活発となっているプリオン病治療開発について臨床研究の成果を紹介する．

変異型CJDと非定型的プリオン病

変異型CJDは他のプリオン病とはことなる特異な臨床・病理像を呈することが知られているものの，発症早期では他の神経精神疾患との鑑別が問題となるばかりでなく，他のプリオン病との鑑別も必要である．WHO（2001年）の変異型CJD診断基準によれば，〔進行性の神経精神症状〕＋〔初期の精神症状，疼痛性感覚症状，失調，ミオクローヌスなどの不随意運動，痴呆のうちの4症状〕＋〔PSDがみとめられない〕であれば，変異型CJDがうたがわれることになる．このことは，精神症状，感覚症状，あるいは失調などを初期症状とする非典型的なプリオン病はすべて変異型CJDの可能性があることになる．

遺伝性プリオン病では，挿入変異型プリオン病（オクタリピート配列の挿入変異），失調型（古典型）GSS（P102L），致死性家族性不眠症（D178N＋129M）などが鑑別にあがるが，他の変異タイプのプリオン病でも129Vや219Kの正常多型を併せ持つ際には，変異型CJDとの鑑別が必要となる可能性がある．遺伝性プリオン病は同一のプリオン蛋白遺伝子型であっても表現型は症例によってばらつきがあり，遺伝的浸透率が低いものが多いことから，診断困難な神経精神症状を呈する例や孤発性プリオン病がうたがわれる例でも，積極的にプリオン蛋白遺伝子解析をおこなう必要がある．

次に，孤発性プリオン病では，従来から古典型あるいはHeidenhain型と呼ばれてきたMM1・MV1型（Parchi分類[1]）の典型的CJD例やMM2大脳皮質型CJD例を除く他のタイプ，すなわちVV1型，MV2型（従来の呼称はKuru斑型），VV2型（従来の呼称は失調型），およびMM2視床型は変異型CJDとの鑑別が必要である．また，医原性CJDの中では非典型的な硬膜移植後CJDには変異型CJDと鑑別を要する症例がある．これらの非典型的なプリオン病では，生前に変異型CJDと鑑別ができず，死後に脳組織から異常型プリオン蛋白を検索しMM2B型でないことを確認してはじめて診断が確定するものもある．

治療に関する臨床研究

変異型CJDや医原性CJDが多発している背景のもと，プリオン持続感染細胞やプリオン病モデルマウスをもちいたプリオン病治療薬開発が活発におこなわれている．これまでに抗プリオン作用が証明されている化合物や薬剤の中で，抗マラリア薬であるキナクリン[2,3]やキニーネ[4]，および抗凝血薬であるペントサンポリサルフェート[5]は患者への応用が実現している．

キナクリン治療，キニーネ治療は，それぞれ本邦のプリオン病患者31例，6例で実施された．キナクリン治療では39%の症例に，キニーネ治療では33%の症例に，投与開始後1〜2週で認知機能などに部分的改善が短期間（1〜4週間）観察され，早い病期の患者で効果発現率が高かった．明らかな生命予後改善効果は観察されなかった．肝機能障害などの副作用による投薬中止はキナクリン治療では68%の症例に，キニーネ治療では50%の症例にみられた．血中濃度解析がおこなわれたキナクリンでは，肝機能障害発生と血中キナクリン濃度に関連がみとめられた．いずれの副作用も可逆的な障害であったが，全身状態が不安定な進行例でキナクリン投与中に死亡した2例がみとめられた．注意深い経過観察と血中濃度モニターにより重篤な副作用は十分に防げると考えられるが，今後のキナクリン・キニーネ治療では，適応を早い病期の症例に絞込む必要がある．また，今回みとめられた効果は，キナクリンの血中濃度が比較的低い治療早期であったことから，低用量投与と肝臓への取り込みを下げるような薬剤との併用を検討する必要がある．

東北大学大学院医学系研究科プリオン蛋白研究部門〔〒980-8575　仙台市青葉区星陵町2番1号〕
（受付日：2004年5月13日）

一方，脳室内ペントサンポリサルフェート持続投与療法は，動物実験での成果を踏まえ，英国の変異型CJD患者1例で臨床試験がおこなわれた．進行期での治療開始であったが，ある程度の効果が観察された．これまでにペントサンポリサルフェートによる副作用はまったく出現していないが，患者で最大効果が期待できる安全投与量を如何に見つけるかが課題である．英国では，この症例の成功を踏まえ，存命中の変異型CJDや遺伝性プリオン病患者（とくに発症早期例）の6症例にも同治療法が実施された．また，ドイツと米国でも各1症例に実施され，フランスでも1症例に実施予定である．複数の患者で同治療法の効果と安全性が確認されることになる．英国と同様に"man-made disease"と呼ばれる後天性プリオン病が多発しているわが国でも，この日本発の治療法を早急に臨床で検討する必要がある．

まとめ

変異型CJDとの鑑別が必要となる非定型的なプリオン病について概説した．また，最近活発になっている治療開発について臨床研究の最新成果を紹介した．

文　献

1) Parchi P, Giese A, Capellari S, et al : Classification of sporadic Creutzfeldt-Jakob disease based on molecular and phenotypic analysis of 300 subjects. Ann Neurol 1999 ; 46 : 224—233
2) Doh-ura K, Iwaki T, Caughey B : Lysosomotropic agents and cysteine protease inhibitors inhibit scrapie-associated prion protein accumulation. J Virol 2000 ; 74 : 4894—4897
3) Korth C, May BC, Cohen FE, et al : Acridine and phenothiazine derivatives as pharmacotherapeutics for prion disease. Proc Natl Acad Sci USA 2001 ; 98 : 9836—9841
4) Murakami-Kubo I, Doh-ura K, Ishikawa K, et al : Quinoline derivatives are therapeutic candidates for transmissible spongiform encephalopathies. J Virol 2004 ; 78 : 1281—1288
5) Doh-ura K, Ishikawa K, Murakami-Kubo I, et al : Treatment of transmissible spongiform encephalopathy by intraventricular drug infusion in animal models. J Virol 2004 ; 78 : 4999—5006

Abstract

Prion diseases : disease diversity and therapeutics

Katsumi Doh-ura, M.D.
Department of Prion Research, Tohoku University Graduate School of Medicine

More than one hundred victims of iatrogenic CJD with cadaveric dura mater grafting have been recognized in Japan, and the people have been also exposed to a risk of outbreaks of variant CJD. These diseases are distinct from other forms of prion diseases as well as other neuropsychiatric disorders, but on an early clinical stage, their differential diagnoses from other atypical forms of prion diseases are not necessarily easy. Thus, atypical forms of prion diseases were overviewed and discussed here. In addition, data on recent clinical trials of enteral antimalarial drug (quinacrine or quinine) treatment or intracerebroventricular pentosan polysulfate treatment were presented and discussed, because research progress in the therapeutics for prion diseases has been remarkably made on the basis of the prevalence of those acquired forms of prion diseases.

(Clin Neurol, 44 : 855—856, 2004)

Key words : variant CJD, differential diagnosis, therapeutics, antimalarial, pentosan polysulfate

Available online at www.sciencedirect.com
SCIENCE DIRECT
Virology 320 (2004) 40–51
VIROLOGY
www.elsevier.com/locate/yviro

Antigenic characterization of an abnormal isoform of prion protein using a new diverse panel of monoclonal antibodies

Chan-Lan Kim,[a] Atsushi Umetani,[b] Toshio Matsui,[b] Naotaka Ishiguro,[a] Morikazu Shinagawa,[a,1] and Motohiro Horiuchi[a,c,*]

[a] *Laboratory of Veterinary Public Health, Obihiro University of Agriculture and Veterinary Medicine, Inada-cho, Obihiro, Hokkaido 080-8555, Japan*
[b] *Obihiro Research Laboratory, Fujirebio Inc., Kawanishi-cho, Obihiro, Hokkaido 089-1111, Japan*
[c] *Research Center for Protozoan Diseases, Obihiro University of Agriculture and Veterinary Medicine, Inada-cho, Obihiro, Hokkaido 080-8555, Japan*

Received 14 July 2003; returned to author for revision 22 October 2003; accepted 22 October 2003

Abstract

We established a panel of monoclonal antibodies (mAbs) against prion protein (PrP) by immunizing PrP gene-ablated mice with the pathogenic isoform of prion protein (PrP^{Sc}) or recombinant prion protein (rPrP). The mAbs could be divided into at least 10 groups by fine epitope analyses using mutant rPrPs and pepspot analysis. Seven linear epitopes, lying within residues 56–90, 119–127, 137–143, 143–149, 147–151, 163–169, and 219–229, were defined by seven groups of mAbs, although the remaining three groups of mAbs recognized discontinuous epitopes. We attempted to examine whether any of these epitopes are located on the accessible surface of PrP^{Sc}. However, no mAbs reacted with protease-treated PrP^{Sc} purified from scrapie-affected mice, even when PrP^{Sc} was dispersed into a detergent–lipid protein complex, to reduce the size of PrP^{Sc} aggregates. In contrast, denaturation of PrP^{Sc} by guanidine hydrochloride efficiently exposed all of the epitopes. This suggests that any epitope recognized by this panel of mAbs is buried within the PrP^{Sc} aggregates. Alternatively, if the corresponding region(s) are on the surface of PrP^{Sc}, the region(s) may be folded into conformations to which the mAbs cannot bind. The reactivity of a panel of mAb also showed that the state of PrP^{Sc} aggregation influenced the denaturation process, and the sensitivity to denaturation appeared to vary between epitopes. Our results demonstrate that this new panel of well-characterized mAbs will be valuable for studying the biochemistry and biophysics of PrP molecules as well as for the immunodiagnosis of prion diseases.

Keywords: Scrapie; Prion; BSE; Monoclonal antibody; Epitope mapping

Introduction

Transmissible spongiform encephalopathies (TSEs), so-called prion diseases, are fatal neurodegenerative diseases including scrapie in sheep and goats, bovine spongiform encephalopathy, and Creutzfeldt–Jakob disease (CJD) in humans (Prusiner, 1991). The causative agent, prion, is thought to be composed solely, if not entirely, of a pathogenic isoform of the prion protein (PrP^{Sc}). PrP^{Sc} is generated from a host-encoded cellular prion protein (PrP^{C}) by certain post-translational modifications including a conformational transformation. Although the two PrP isoforms share the same primary structure (Hope et al., 1986), PrP^{Sc} is distinguished from PrP^{C} by biochemical and biophysical properties such as high β-sheet content (Pan et al., 1993; Safar et al., 1993), partial resistance to protease digestion, and insolubility in nonionic detergent (Meyer et al., 1986). The conformational transformation from PrP^{C} to PrP^{Sc} requires preexisting PrP^{Sc} as a template and is thought to be a central event in PrP^{Sc} formation and prion replication. However, the molecular mechanism of the conformational transformation remains unclear. To elucidate the mechanism, structural information from two PrP isoforms is needed. At this time, the NMR structure of a recombinant PrP resembling PrP^{C} has been determined (Riek et al., 1996), whereas the structure of PrP^{Sc} is not yet known.

* Corresponding author. Laboratory of Prion Diseases, Graduate School of Veterinary Medicine, Hokkaido University, Kita 18, Nishi 9, Kita, Sapporo 060-0818, Japan. Fax: +81-11-706-5293.
E-mail address: horiuchi@vetmed.hokudai.ac.jp (M. Horiuchi).
[1] Present address: Prio Disease Research Center, National Institute of Animal Health, Kannondai, Tsukuba, Ibaragi, 305-0856, Japan.

0042-6822/$ - see front matter © 2004 Elsevier Inc. All rights reserved.
doi:10.1016/j.virol.2003.10.026

A diverse panel of anti-PrP mAbs is invaluable for analyzing the difference between PrP^C and PrP^{Sc}, as well as for the biochemical and structural analysis of PrP molecules. To date, many monoclonal antibodies (mAbs) against PrP have been generated by immunizing with PrP^{Sc} purified from scrapie-affected animals (Barry and Prusiner, 1986; Kascsak et al., 1987; Williamson et al., 1996), recombinant PrP (Zanusso et al., 1998), synthetic PrP peptides (Harmeyer et al., 1998; Horiuchi et al., 1995; O'Rourke et al., 1998), or a PrP expression plasmid (Krasemann et al., 1996). Most of the anti-PrP antibodies developed so far react with linear or discontinuous epitopes on PrP^C and recombinant PrP molecules, as well as with PrP^{Sc} treated with denaturant. These types of anti-PrP antibodies are now widely used for the immuno-detection of PrP^{Sc}. Because these antibodies themselves cannot distinguish the two PrP isoforms when the molecules are treated with denaturant, proteolytic removal of PrP^C before immuno-staining is essential for the detection of PrP^{Sc} by immunoblotting or enzyme-linked Immunosorbent assay (ELISA). One mAb, designated 15B3, generated by immunizing PrP gene-deficient mice with recombinant bovine PrP, was reported to recognize a PrP^{Sc}-specific conformational epitope consisting of two PrP molecules (Korth et al., 1997). However, further characterization of this mAb has not been published. Recent reports also describe mAbs that appear to recognize discontinuous epitopes on PrP^C but do not appear to react with PrP^{Sc} (Yokoyama et al., 2001).

Further PrP^{Sc}- and PrP^C-specific antibodies, as well as additional characterized antibodies to PrP molecules, will help to elucidate the structure–function relationships of PrP, structural differences between PrP^C and PrP^{Sc}, and mechanisms of conformational transformation. In addition, new antibodies showing higher reactivity and specificity than those currently available would help to improve the sensitivity of PrP^{Sc} detection. Although a large number of antibodies against PrP have been generated, it is possible that undefined epitopes still exist. In this study, we established a panel of mAbs that covers diverse epitopes on the mouse PrP molecules by immunizing $PrP^{-/-}$ mice with either recombinant mouse PrP or PrP^{Sc} purified from scrapie-affected mouse brains. The mAbs could be at least divided into 10 groups based on fine epitope mapping. Finally, we discuss how this panel of well-characterized mAbs will be useful for analyzing the molecular properties of PrP as well as for diagnostic purposes.

Results

Production of monoclonal antibodies against PrP molecules

For the immunization of PrP gene-ablated mice, we prepared rMoPrP as well as PrP^{Sc} from brains of scrapie-affected mice. Fig. 1 shows the purity of rMoPrP and PrP^{Sc}. rMoPrP23–231 expressed by pRSETB in *E. coli* formed inclusion bodies (Fig. 1A). The rMoPrP23–231 recovered from inclusion bodies was dissolved with 6 M GdnHCl, and further purified with Ni^{2+}-charged IMAC. After dialysis, rMoPrP possessing an intramolecular disulfide bond was

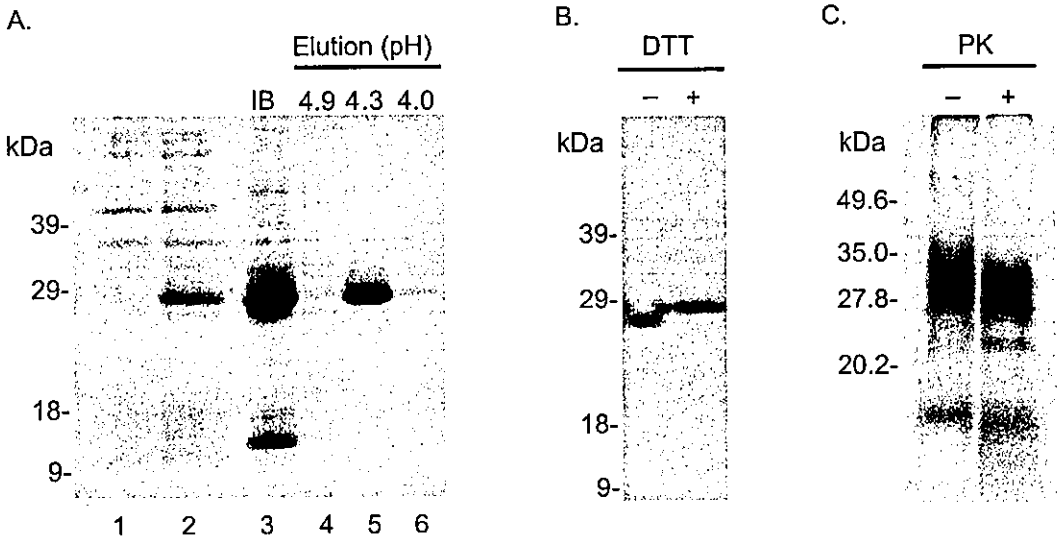

Fig. 1. Purity of rPrP and PrP^{Sc}. (A) Purification of rPrP from bacterial lysates. Whole lysates of *E. coli* transformed with pRSETB (lane 1) and pRSETB/MoPrP23–231 (lane 2) after induction with IPTG for 2 h. Inclusion bodies were prepared from whole bacterial lysates (lane 3) for partial purification of rPrP. Inclusion bodies were dissolved in 6 M GdnHCl and applied to Ni^{2+}-charged IMAC. The rPrP was eluted with a stepwise pH gradient (lanes 4–6), and rPrP eluted at pH 4.3 was dialyzed against acetate buffer to remove GdnHCl. (B) Formation of intramolecular disulfide bonds. After the dialysis, rPrP possessing an intramolecular disulfide bond was collected by reverse-phase HPLC. DTT + and – indicates purified rPrP dissolved with sample buffer with and without 100 mM DTT. (A and B) Coomassie blue staining. (C) Purity of PrP^{Sc} fraction from scrapie-affected mouse brains. The PrP^{Sc} fraction treated (+) and untreated (–) with PK was visualized by sliver staining and the purity was estimated by densitometric analysis by using Atto Densitograph (Atto Co. Ltd.). Molecular mass markers are in kilodaltons (kDa).

collected by reverse-phase HPLC (Fig. 1B). The $MoPrP^{Sc}$ prepared from brains of scrapie-affected mice was estimated to be >70% pure even without PK treatment (Fig. 1C), and a bioassay revealed that this fraction was estimated to contain more than10^{11} LD_{50}/mg from our dose–incubation time standard curve for Obihiro strain (data not shown). These PrP fractions were used for immunization of PrP gene-ablated mice, and splenocytes from immunized mice were fused with myeloma cells. Hybridomas positive for both rMoPrP and $MoPrP^{Sc}$, or those positive either for rMoPrP or $MoPrP^{Sc}$, were selected. Finally, we established 4, 10, and 15 hybridomas using rMoPrP23–231, rMoPrP89–231 or $MoPrP^{Sc}$, respectively, as the immunogen (Table 1).

Epitope analyses

To determine the epitopes recognized by the mAbs, we first examined their reactivity to various mutant rPrPs by ELISA. Based on their reactivity, the mAbs were divided into seven groups (Table 1). The mAbs in group I did not react with rMoPrP lacking the N-terminal region, indicating that their epitopes are located in residues 23–89. Group II mAbs reacted with all rMoPrPs except for rMoPrP155–231, indicating that they recognize the regions between residues 89 and 155. Group III consists of mAb 43C5, which reacted with all rMoPrPs, suggesting that its epitope is located between residues 155 and 167. The mAbs in group IV did not react with mutants lacking the C-terminus but reacted with other mutants, indicating that they recognize the epitopes on the C-terminal part of PrP molecule. The mAbs in group V reacted with rMoPrP155–231 but not with rMoPrP23–214. In addition, these mAbs did not react with point mutants rHaPrPC179A and rHaPrPC214A in which the cysteines at residues 179 and 214, respectively, were replaced with alanine. The mAbs reacted equally with rMoPrP23–231 and rHaPrP23–231 (data not shown), indicating amino acid differences between Mo and HaPrP did not influence the reactivity. These facts suggest that mAbs in groups V recognize discontinuous epitopes, including the region within residues 155–231, and that the epitopes are dependent on the intramolecular disulfide bond in the PrP molecule. The mAbs in group VI reacted with rMoPrP89–231, but neither reacted with rMoPrP155–231 nor point mutants of rHaPrP, suggesting that the epitope for these mAbs include the region within residues 89–231 and also are dependent on the intramolecular disulfide bond. The reactivity of mAb 72 (group VII) was difficult to figure out the epitope. It reacted with rMoPrP89–231 and 23–167, suggesting that the epitope is located within residues 89–167. However, the mAb did not react with rMoPrP23–214, rHaPrPC179A, or rHaPrPC214A, but reacted with rHaPrP23–231, again suggesting that the epitope depends on the presence of the intramolecular disulfide bond.

Further precise epitope mapping was carried out by pepspots analysis (Fig. 2). The reactivity of the group I mAbs revealed that they recognize a portion of octa-peptide repeat in N-terminus, although there is some difference in the amino acid sequence recognized by these mAbs. Based on the reactivity (Fig. 2A), the epitope for mAb 8 was WGQPHG at aa 56–61, 64–69, 72–77, and 80–85. mAbs 110 and 37 reacted with peptides 16–19 and 28–31, indicating that the recognized sequence is PHGGGWG at aa 59–65 and 83–89 (Fig. 2B). mAbs 40, 106, and 162 showed broad reactivity to peptides ranging from 13 to 33 (Fig. 2C). The reaction to peptides including 17 to 19 and 29 to 33 the most intense, suggesting that the major recognition sequence for these mAbs is PHGGGWGQ at aa 59–66 and 83–90, although the minimum required sequence appears to be WGQ. The group II mAb 132 reacted with peptides from 47 to 49, which share residues

Table 1
Grouping of mAbs based on the reactivity to rPrP deletion and point mutants

Group	mAb[a] (Isotype[b])	rPrP used as antigen[c]					
		rMoPrP23–167	rMoPrP23–214	rMoPrP89–231	rMoPrP155–231	rHaPrPC179A	rHaPrPC214A
I	8(2b), 37(2b), 40(2b), 106(2b), 110(2b), 162(2a)	+	+	–	–	+	+
II	13(2b), 32(2a), 118(2b), 132(G1), 149(2b), 31C6(G1)	+	+	+	–	+	+
III	43C5(G1)	+	+	+	+	+	+
IV	39(2b), 147(2b)	–	–	+	+	+	+
V	66(G1), 31B1(G1), 31B5(G1), 42B4(G1), 42D2(G1), 42D6(G1), 44A2(G1), 44A5(G1), 44B1(2a), 44B5(G1)	–	–	+	+	–	–
VI	23D9(G1), 42D3(G1), 44B2(G1)	–	–	+	–	–	–
VII	72(G1)	+	–	+	–	–	–

[a] MAbs named only with numbers were obtained by using $MoPrP^{Sc}$ as the immunogen, others named with a combination of numbers and letters were obtained using rMoPrP as the immunogen Among the latter, mAbs starting with 23 or 31, and 42, 43 or 44 were obtained by immunization with rMoPrP23–231 and rMoPrP89–231, respectively.
[b] G1, IgG1; 2a, IgG2a; 2b, IgG2b.
[c] Examined by ELISA.

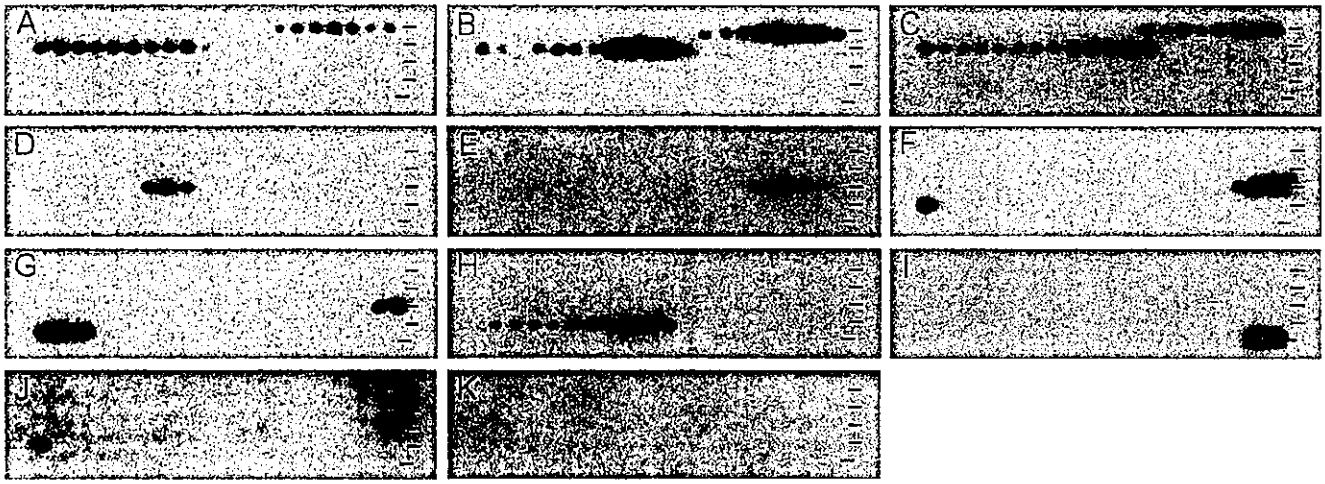

Fig. 2. Pepspot analysis. Bars on the right sides indicate lines of peptide spots. The first through fourth lines contain 20 spots per line, while fifth line contains 19 spots. (A) mAb 8 (group I); (B) mAb 110 (group I); (C) mAb 162 (group I); (D) mAb 132; (group IIa); (E) mAb 118 (group IIb); (F) mAb 31C6 (group IIc); (G) mAb 32 (group IId); (H) mAb 43C5 (group III); (I) mAb 147 (group IV); (J) mAb 72 (group VII); (K) mAb P1–284 (anti-parvovirus mAb, negative control).

119–127, AVVGGLGGY (Fig. 2D). mAbs 13 and 118 (group II) reacted with peptides from 55 to 58, which contain the fragment corresponding to residues 137–143, MIHFGND (Fig. 2E). The mAb 31C6 (group II) reacted with peptides from 58 to 61, which share in common residues 143–149, DWEDRYY (Fig. 2F). mAbs 32 and 149 (group II) reacted with five peptides from 59 to 63 that share a common sequence RYYRE, residues 147–151 (Fig. 2G). The mAb 43C5 (group III) reacted with 10 continuous spots but intense reactivity was observed to four peptides from 68 to 71, which contain the fragment corresponding to residues 163–169, RPVDQYS (Fig. 2H). This result is consistent with the epitope analysis of mutant recombinant PrPs. mAbs 39 and 147 (group IV) reacted with peptides 98 and 99, which correspond to the extreme C-terminus of PrP molecules, residues 219–229, KESQAYYDGRR (Fig. 2I). The mAbs in groups I–IV reacted with rHaPrPC179A and rHaPrPC214A in the ELISA (Table 1) and PrP^{Sc} in immunoblot analysis (Fig. 3), indicating that these mAbs recognize linear epitopes. mAb 72 appeared to recognize discontinuous epitope based on the reactivity to mutant rPrP (Table 1), although the mAb reacted with peptides 60 and 61, which share residues 143–153 (Fig. 2J).

Based on the fine epitope mapping by pepspot analysis, the mAbs in group II of Table 1 can be separated into four groups, designated IIa–IId. Together, the mAbs produced in this study can be divided into at least 10 groups; 7 that recognize linear epitopes, and 3 that recognize discontinuous epitopes (Table 2).

Species specificity of mAbs

We next examined the specificity of the mAbs by ELISA using species-specific versions of rMoPrP, rHaPrP, rShPrP, and rBoPrP. Most of the mAbs reacted with the rPrP from all four species (hamster, bovine, mouse and ovine), while the following mAbs showed obvious species-specific reactivity: mAbs 13 and 118 in group IIb, mAbs 39 and 147 in group IV, and mAb 66 reacted to Mo and HaPrP, while mAbs 42D2 and 44B5 showed intense reaction to Mo and HaPrP, moderate reaction to ShPrP but no reaction to BoPrP (data not shown).

Fig. 3 shows the reactivity to $MoPrP^{Sc}$, ovine PrP^{Sc} ($ShPrP^{Sc}$), and bovine PrP^{Sc} ($BoPrP^{Sc}$) in immunoblot analysis. mAbs 110, 132, 118, 31C6, 32, 43C5, and 147, which recognize linear epitopes, reacted with PrP^{Sc} prepared from brains of the disease-affected animals. Surprisingly, mAbs 44B1 and 72, which appeared to recognize discontinuous epitopes, showed an intense reaction to PrP^{Sc} in immunoblotting. The species-specific reactivities of mAbs 132, 118, 32, 43C5, 147, 44B1, and 72 are consistent with the results from ELISA; mAbs 118 and 147 only reacted with $MoPrP^{Sc}$ while other mAbs reacted with PrP^{Sc} from the other three species. In contrast to the results from ELISA, mAb 31C6 only reacted with $MoPrP^{Sc}$ and mAb 110 reacted with Mo and $ShPrP^{Sc}$ but not with $BoPrP^{Sc}$ in immunoblot analysis.

Reactivity of panel mAbs to purified PrP^{Sc}

To determine whether any of the antibody-reactive epitopes are exposed in the infectivity-associated PrP^{Sc}, we examined the reactivity of mAbs to purified $MoPrP^{Sc}$ by ELISA. A set of three PrP^{Sc} preparations, PK-untreated and non-denatured, PK-treated and non-denatured, and PK-treated and denatured, was used for each mAb (Fig. 4). All the mAbs reacted with PK-untreated non-denatured PrP^{Sc}, although the reactivity was lost when PrP^{Sc} was treated with PK. However, the mAbs regained reactivity when the PK-treated PrP^{Sc} was denatured with GdnHCl. These results suggest that the inability of the antibodies to react to PK-

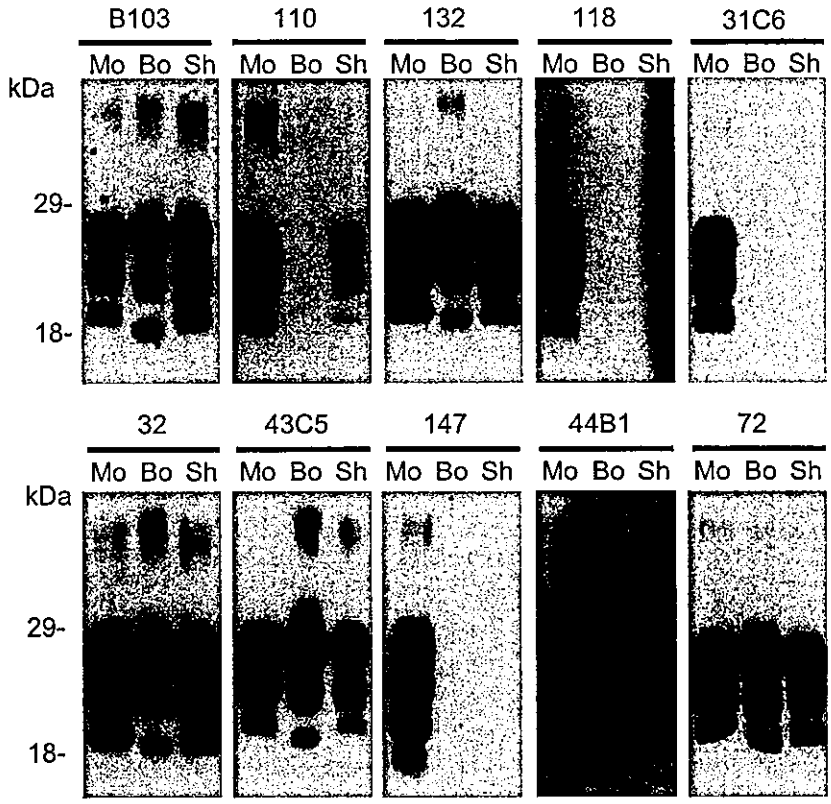

Fig. 3. Species specificity in Western blot analysis. Crude preparations of mouse (Mo), bovine (Bo), and sheep (Sh) PrP^{Sc} were prepared as described elsewhere (Grathwohl et al., 1997) and were separated by SDS-PAGE and transferred onto PVDF membranes. Brain tissue equivalents of 25 mg, 500, and 125 μg were loaded for Mo, Bo, and Sh PrP^{Sc}, respectively. The blots were stained with B-103 rabbit polyclonal antibodies (Horiuchi et al., 1995) or mAbs as indicated.

treated PrP^{Sc} is not due digestion of the PrP^{Sc}. Rather, it appears that the epitopes on PK-treated PrP^{Sc} are cryptic. A considerable amount of PK-sensitive PrP, including PrP^{C}, is co-purified during PrP^{Sc} purification in the absence of PK treatment (Caughey et al., 1995). Therefore, it is likely that reaction of the mAbs with PK-untreated non-denatured PrP^{Sc} accounts for the reaction to PK-sensitive PrP that exposes these epitopes on its accessible surface. Furthermore, the epitopes recognized by our panel of mAbs do not appear to be exposed on the surface of the PK-resistant core

Table 2
Characterization of mAbs against PrP

Group	mAb	Epitope[a]		Reactivity to PrP^{Sc} in ELISA[b]		
		position (amino acid)	L/DC	PK(−) GdnHCl(−)	PK(+) GdnHCl(−)	PK(+) GdnHCl(+)
I	8, 37, 40, 106, 110, 162	56–90	L	+	−	+
IIa	132	119–127	L	+	−	+
IIb	13, 118	137–143	L	+	−	+
IIc	31C6	143–149	L	+	−	+
IId	32, 149	147–151	L	+	−	+
III	43C5	163–169	L	+	−	+
IV	39, 147	219–229	L	+	−	+
V	66[c], 31B1, 31B5, 42B4, 42D2, 42D6, 44A2, 44A5, 44B1, 44B5[c]	155–231	DC	+(−)[c]	−	+(−)[c]
VI	23D9, 42D3, 44B2	89–231	DC	+	−	+
VII	72	89–231 (143–153)	DC	+	−	+

[a] L, linear epitope; DC, discontinuous epitope.
[b] Treatments of PrP^{Sc} are as described in Fig. 4.
[c] MAbs 66 and 44B5 reacted with rPrP but did not react with the three PrP^{Sc} preparations.

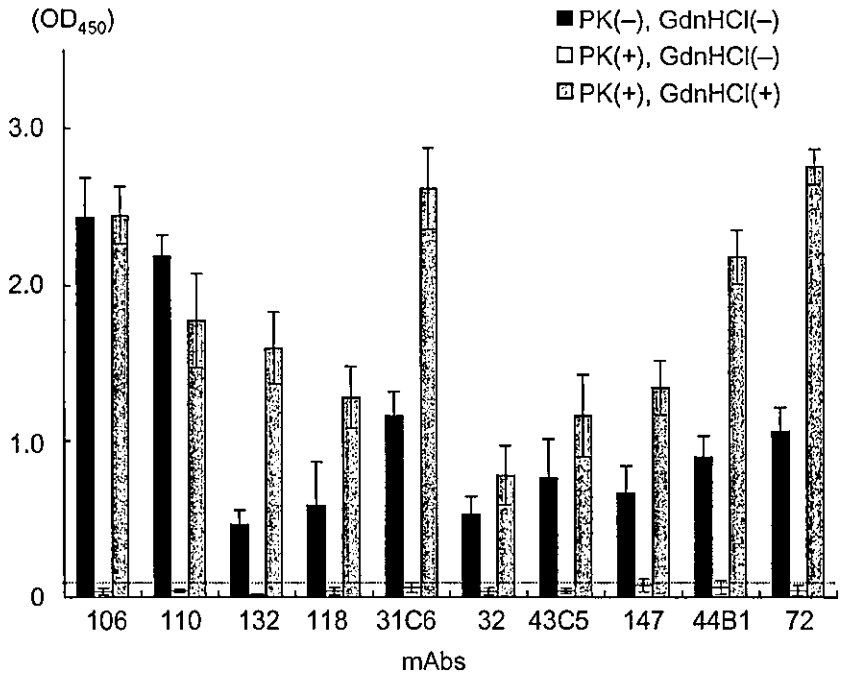

Fig. 4. Reactivity of mAbs to PrP^{Sc} fraction in ELISA. A set of three wells were used for each mAb: after the adsorption of purified PrP^{Sc} fraction, first well was neither treated with PK nor with GdnHCl [PK(–), GdnHCl(–)], second well was treated with 40 μg/ml PK for 60 min at 37 °C [PK(+), GdnHCl(–)], and third well was treated with PK and then further treated with 6M GdnHCl for 60 min to denature PrP^{Sc} [PK(+), GdnHCl(+)]. mAbs indicated in the figure were used as a representative for each group in Table 2. Dotted line indicates the cut-off value [An average OD_{450} value of negative control monoclonal antibody plus 5 times standard deviation ($n > 4$)].

of PrP^{Sc}. Instead, they become accessible to the mAbs after denaturation of PK-resistant core of PrP^{Sc}.

Reduction of PrP^{Sc} aggregate size does not expose cryptic epitopes

Purified PrP^{Sc} forms relatively large aggregates that can be precipitated by centrifugation at 10000 × *g*. We were concerned that the large aggregates themselves affect the antibody accessibility to PrP^{Sc}. To address this concern, we attempted detergent-lipid-protein complex (DLPC) treatment, which can reduce aggregate size without loss of infectivity (Gabizon et al., 1987). As shown in Fig. 5, nearly all of the purified PrP^{Sc} was present in the pellet after centrifugation at 10000 × *g* for 10 min, although more than the half of DLPC-treated PrP^{Sc} remained supernatant. Further centrifugation at 100000 × *g* of the soluble DLPC-treated PrP^{Sc} resulted in its precipitation. These results show that the DLPC treatment reduces the size of PrP^{Sc} aggregates without significant a loss of PK resistance. As described above (Fig. 4), mAbs did not react with PK-treated, DLPC-untreated PrP^{Sc} unless it was denatured (at 0 M GdnHCl in Fig. 6). Although all the mAbs except for mAbs 110, 132, and 32 faintly reacted with DLPC-treated PrP^{Sc} without denaturation (OD_{450} < 0.17 at 0 M GdnHCl), none of the mAbs showed a significant increase in reactivity to DLPC-treated PrP^{Sc} compared with DLPC-untreated PrP^{Sc}. These results suggest that the reduction of aggregate size by DLPC is not sufficient to expose cryptic epitopes on PrP^{Sc}.

Exposure of cryptic epitopes by denaturation

The reduction of PrP^{Sc} aggregate size by DLPC did not result in the efficient exposure of the hidden epitopes. In

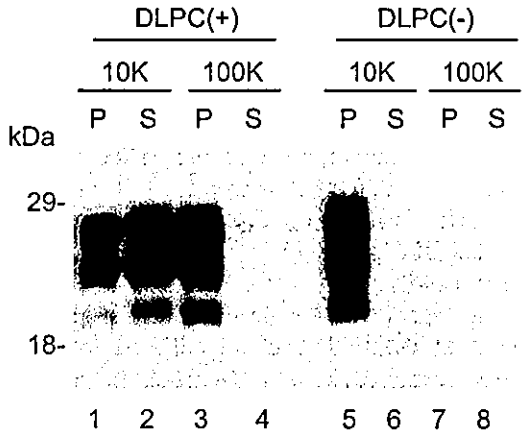

Fig. 5. Sedimentation analysis of DLPC-treated PrP^{Sc}. DLPC-treated (lanes 1–4) and untreated PrP^{Sc} (lanes 5–8) were digested by PK and then subjected to sedimentation analysis. Centrifugation at 10000 × *g* yielded pellet (lanes 1 and 5) and supernatant (lanes 2 and 6) fractions. The supernatants were further subjected to ultracentrifugation at 100000 × *g* to generate pellet (lanes 3 and 7) and supernatant (lanes 4 and 8). The PrP^{Sc} in each fraction was detected by immunoblot analysis.

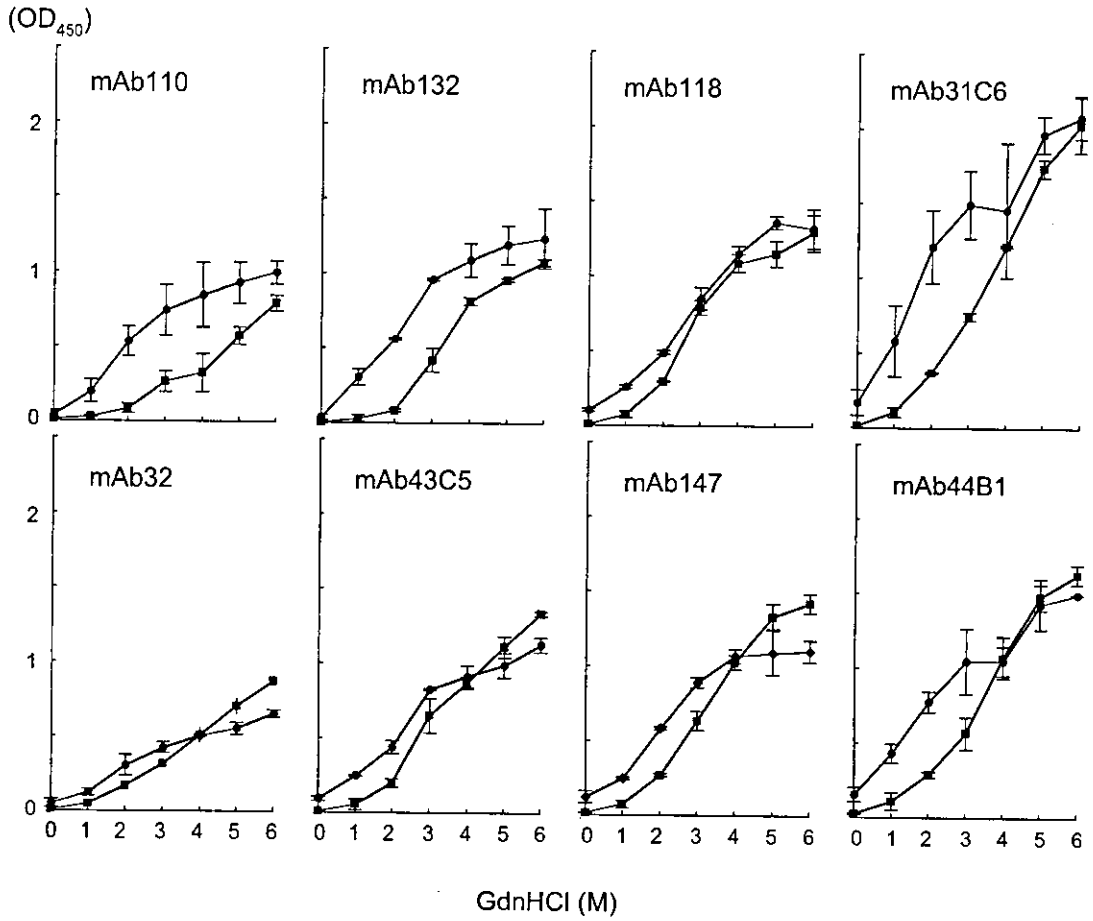

Fig. 6. Exposure of epitopes by GdnHCl treatment. DLPC-treated or untreated PrP^{Sc} was adsorbed to an ELISA plate, digested with PK, and then treated with the various concentrations of GdnHCl indicated at the bottom of the figure. Average and SD of three independent experiments were plotted. Circles indicate the DLPC-treated PrP^{Sc}, whereas squares indicate DLPC-untreated PrP^{Sc}.

contrast, Fig. 6 shows that treatment with of both PrP^{Sc} preparations to GdnHCl dramatically increased the reactivities to all mAbs. This indicates that the dissociation and denaturation of PrP^{Sc} aggregates resulted in pronounced exposure of epitopes. However, one striking difference in the reactivity of mAbs was observed especially at lower GdnHCl concentration: most of the mAbs displayed a higher reactivity to DLPC-treated PrP^{Sc} than to DLPC-untreated PrP^{Sc} at the lower GdnHCl concentrations. This suggests that DLPC-treated PrP^{Sc} may be more sensitive to denaturant than DLPC-untreated PrP^{Sc}.

PrP^{Sc} aggregates are thought to undergo partial denaturation in 2 M GdnHCl, and are believed to be almost completely denatured in 6 M GdnHCl. In parallel with denaturation of PrP^{Sc}, 2 M GdnHCl treatment does not completely abolish prion infectivity, although >4 M GdnHCl treatment drastically reduces the infectivity (Caughey et al., 1997; Prusiner et al., 1993). Table 3 shows the ratio of OD_{450} (in Fig. 6) at 2 and 6 M GdnHCl for both PrP^{Sc} preparations. In DLPC-untreated PrP^{Sc}, the ratios varied from 0.08 to 0.19, suggesting that less than 20% of the epitope for each mAb was exposed following 2 M GdnHCl treatment. In contrast, the ratios increased, varying from 0.37 to 0.58, following DLPC treatment, indicating that the reduction of PrP^{Sc} size influences the sensitivity to denaturation. The variation of the ratios may reflect the difference in the denaturation process for the specific epitopes. For example, epitopes for mAbs 118 and 43C5 appeared to be more resistant to denaturation by GdnHCl than other epitopes.

Table 3
Reactivity of mAbs to partially denatured PrP^{Sc}

mAb	DLPC-untreated		DLPC-treated	
	OD_{450} at 2M/6M GdnHCl	Ratio	OD_{450} at 2M/6M GdnHCl	Ratio
110	0.084/0.789	0.10	0.529/0.994	0.53
132	0.084/1.074	0.08	0.560/1.235	0.45
118	0.295/1.292	0.19	0.488/1.320	0.37
31C6	0.367/2.031	0.18	1.211/2.085	0.58
32	0.167/0.872	0.19	0.305/0.653	0.47
43C5	0.199/1.332	0.15	0.438/1.123	0.39
147	0.271/1.419	0.19	0.581/1.099	0.53
44B1	0.290/1.628	0.18	0.775/1.492	0.52

Discussion

To generate a diverse panel of mAbs to PrP molecules, we established a variety of hybridomas by using rMoPrP and $MoPrP^{Sc}$ purified from scrapie-affected mice brain as immunogens. According to the extensive epitope analyses using rPrP and pepspot membrane, our mAb panel contained mAbs recognizing at least seven different linear epitopes and three discontinuous epitopes. Five of seven linear epitopes were located within the N-terminal half of the PK-resistant core of PrP^{Sc} (aa 119–127, 137–143, 143–149, 147–151, and 163–169). This region is thought to undergo a major conformational change from random coil or α-helix- to β-sheet-rich structure during the conversion of PrP^{C} to PrP^{Sc}. Among the antibodies, mAb 132, recognizing the epitope aa 119–127 (AVVGGLGGY), is of particular interest. This region is adjacent to the highly amyloidogenic sequence AVAAAAVA (aa 112–119) (Gasset et al., 1992) and the first short β-strand (aa 128–131). Studies have shown that this region plays an important role in the conversion of PrP^{C} to PrP^{Sc} (Holscher et al., 1998; Muramoto et al., 1996). In addition, this region is highly conserved between mammals and birds, suggesting the importance of this region in PrP^{C} biology (Wopfner et al., 1999). Thus, mAb 132 will facilitate studies of how this region is involved in the conversion process as well as how PrP^{C} functions. The epitope for mAb 43C5 (aa 163–169) on PrP^{C} is of also interest because this region, in conjunction with its C-terminal portion, is thought to be a binding domain for an unidentified factor tentatively named protein X, which is expected to act as a molecular chaperon during the conversion process (Kaneko et al., 1997). mAb 43C5 will also be a good tool for studying how this region is involved in the intermolecular interaction. In addition, the first α-helix on PrP^{C} may undergo α to β conformational change during the conversion process, although this has not been fully clarified (Zhang et al., 1995). The mAbs in groups IIb, IIc, and IId recognizing the first α-helix and its immediate N-terminal portion will therefore contribute to understanding of structural differences in this region.

Elucidation of the PrP^{Sc} structure is an important problem to understand the identity of prion. Although the model structure of PrP^{Sc} and its aggregates were recently proposed from electron crystallography (Wille et al., 2002), their atomic structures remain to be elucidated. Studies of antibody accessibility will help to clarify PrP^{Sc} structure (Kanyo et al., 1999). Our mAbs did not show intense reactivity to PK-treated PrP^{Sc}, which is associated with prion infectivity, although they strongly react with PrP^{Sc} after denaturation. This suggests none of the epitopes recognized by our mAb panel are accessible by mAbs on PrP^{Sc} aggregates. The epitope at the C-terminus of PrP^{Sc} is reported to be accessible to antibody (Peretz et al., 1997; Williamson et al., 1998). In that study, the authors used DLPC treatment, which can disperse the PrP^{Sc} aggregates into liposome and reduce particle size of PrP^{Sc} aggregates (Gabizon et al., 1987). Although we confirmed that DLPC treatment could reduce the PrP^{Sc} aggregate size, some mAbs including one recognizing the C-terminus showed a trace of reactivity even when we used DLPC-treated PrP^{Sc}. In contrast, denaturation of DLPC-treated PrP^{Sc} was required to expose the cryptic epitopes. This implies that DLPC treatment might not be sufficient to expose the cryptic epitope(s) on PrP^{Sc}. There are some differences in experimental conditions between our investigations and those of Peretz et al. that could explain the differences in our results. First, they used Sc237 hamster scrapie, while we used the Obihiro strain of mouse-adapted scrapie. Second, preparation of PrP^{Sc} for ELISA also varied. Peretz et al. treated PrP^{Sc} with PK and the resulting PrP^{27-30} was dispersed into liposomes. In contrast, we performed DLPC treatment first after which DLPC-treated PrP^{Sc} was digested with PK to eliminate PK-sensitive PrP, which is expected to possess some exposed epitopes. Third, they used streptavidin-coated plates to immobilize the PrP^{Sc} after biotinylation, while, in this study, we directly adsorbed PrP^{Sc} to the ELISA plate by possible hydrophobic interaction. Finally, the antibodies used in the two studies were different. Although pepspot analysis demonstrated that mAbs 39 and 147 recognize an extreme C-terminal part of PrP, we used purified IgG instead of a smaller single-strand Fab fragment. We do not know the reason for the difference in the mAb reactivity to the C-terminus in our results and those reported by Peretz et al., it is conceivable that these differences in the experimental conditions might influence the results.

Denaturation of PrP^{Sc} aggregates caused the exposure of cryptic epitopes (Serban et al., 1990; Williamson et al., 1996). Here we observed that the sensitivity to denaturant varies between the epitopes. In DLPC-treated PrP^{Sc}, the epitopes for mAb 118 and 43C5 appeared to be more resistant to denaturation as determined by the ratio of OD at 2 to 6 M GdnHCl treatment. This difference implies complexity in the inter- or intramolecular interactions involved in the formation of PrP^{Sc} aggregates. It is of particular interest to examine what kind of inter- or intramolecular interactions determine prion infectivity or if exposure of certain epitopes correlates to prion inactivation. Our data also showed that the DLPC-treated PrP^{Sc} is more sensitive to denaturant than DLPC-untreated PrP^{Sc}, indicating that prion inactivation methods are possibly influenced by the state of PrP^{Sc} aggregation and environment.

The epitopes for mAbs raised against rPrP seemed to be relatively restricted, and 9 of 14 mAbs recognized a discontinuous epitope within aa 155–231, indicating this epitope on rPrP was immunodominant in $PrP^{-/-}$ mice. In contrast, the epitopes for the mAbs raised against PrP^{Sc} broadly spanned the PrP molecules. Furthermore, 13 of 14 hybridomas from mice immunized with rPrP secreted IgG1, although hybridomas secreting IgG2b were predom-

inantly established from mice immunized with PrP^{Sc} (9 of 15). Therefore, the differences in the immunodominant regions and predominant immunoglobulin subtypes suggest that the two PrP preparations elicited different type of immune responses, although the two PrPs share primary structure and we used the same immunization procedure. Although PrP^{Sc}-specific antibodies are thought to be an attractive tool for analyzing properties of PrP^{Sc} as well as establishing new diagnostic methods, only one has been previously reported (Korth et al., 1997). Thus, the unique immune response against the PrP^{Sc} fraction suggests that the use of an infectivity-associated PrP^{Sc} fraction as an immunogen may help to generate PrP^{Sc}-specific antibodies. In addition, it is still possible that certain regions are located on the surface of PrP^{Sc} as either a linear epitope or as a PrP^{Sc}-specific discontinuous epitope. Actually, Paramithiotis et al. very recently reported that three amino acid residues, YYR, possibly located in the second β-strand, is not antibody accessible on PrP^{C}, although the region is exposed on the surface of PrP^{Sc} (Paramithiotis et al., 2003). Further generation of mAbs, especially those specific to PrP^{Sc}, will be required for determining the surface structure of PrP^{Sc}.

BSE and vCJD are now global concerns. Because therapeutics for prion diseases are not currently available, elimination of prion-contaminated foodstuff and biomedical materials is essential for preventing further spread of the disease. We have found that some of our mAbs possessed higher sensitivity for detecting bovine PrP^{Sc} than some commercial-based anti-PrP mAbs, including 6H4 (data not shown). Further generation of anti-PrP antibodies with higher affinity and avidity will contribute to enhance the sensitivity of PrP^{Sc} detection methods.

Materials and methods

Plasmid construction

The prokaryotic expression vectors pET22b(+) (Novagen) and pRSETB (Invitrogen) were used in these studies. For the construction of expression plasmids based on pET22b(+), cDNA encoding mouse (Mo) PrP codons 23–231 was amplified by PCR with primers MPrP2 and MPrP3, and genomic DNA encoding sheep (Sh) PrP codons 25–234 was amplified with primers SPrP102 and SPrP103. Amplified fragments were cloned into the *Eco*RV site of pBluescript KS(+) (Stratagene) to confirm nucleotide sequences. The cloned fragments were excised by *Msc*I and *Eco*RI digestion and ligated into the corresponding sites of pET22b(+).

For the construction of expression plasmids based on pRSETB, cDNA encoding MoPrP codons 23–231 was amplified with primers MPrP5 and MPrP3. To express deletion mutants of MoPrP aa 23–167, 23–214, 89–231, and 155–231, we used primer sets of MPrP5 and MPrP9, MPrP5 and MPrP11, MPrP10 and MPrP3, and MPrP12 and MPrP3, respectively, were used for PCR. Hamster (Ha) PrP cDNA encoding codons 23–231, ShPrP gene encoding codons 25–234, and bovine (Bo) PrP cDNA encoding codons 25–242 were amplified with primer sets of MPrP5 and MPrP9, SPrP101 and SPrP102, and BPrP101 and BPrP103, respectively. Amplified fragments were digested with *Bam*HI and *Eco*RI and cloned into the *Bam*HI and *Eco*RI sites of pRSETB. Nucleotide sequences of the cloned PrP gene fragments were confirmed before their expression. To generate the mutant HaPrP containing a single amino acid substitution at codon 179 (Cys to Ala) or 214 (Cys to Ala), we used the ExSite PCR-based site-directed mutagenesis kit (Stratagene) according to the supplier's instructions. Primer sets of HPrP1 and HPrP2, and HPrP3 and HPrP4 were used to introduce the nucleic acid substitution encoding codons 179 and 214, respectively. Primer sequences Primer sequences were as follows: MPrP2, 5′-AATGGCCA AAAAGCGGCCAAAGCCTGGA-3′; MPrP3, 5′-GAGAATTCAGCTGGATCTTCTCCCGTCGT-3′; MPrP5, 5′-AAGGATCC GAAAAAGCGGCCAAAGCCTGG-3′; MPrP9: 5′-GAGAATTC TACTGATCCACTGGCCTG-GTAG-3′; MPrP10, 5′-AAGGATCC GGGCCAAG-GAGGGGGTACCCATAATC-3′; MPrP11, 5′-GAGAAT TC AGACGCACATCTGCTCCACCAC-3′; MPrP12, 5′-AAGGATCC GCGCTACCCTAACCAAGTGTACT-3′; SPrP101, 5′-AAGGATCC GAAGAAGCGACCAA-AACCTGGCGG-3′; SPrP102, 5′-TTGAAT TC AACTTGCCCCCCTTTGGTAATAAG-3′; SPrP103, 5′-AATGGCCA AGAAGCGACCAAAACCTGGCGG-3′; BPrP101, 5′-AAGGATCC GAAGAAGCGAC-CAAAACCTGGAGG-3′; BPrP103, 5′-TTGAAT TCA ACTTGCCCCTCGTTGGTAATAAG-3′; HPrP1, 5′-CAC-GAT*GC*TGTCAACATCACCATCAAG-3′; HPrP2, 5′-CACAAAGTTGTTCTGGTTGTTGTACTG-3′; HPrP3, 5′-AGATG*GC*TACCACCCAGTATCAGAAGG-3′; HPrP4, 5′-GCTCCACCACGCGCTCCATTATCTTG-3′(underlines indicate restriction sites used for cloning, bold indicates stop codons, and italics indicate nucleotide substitutions for the mutation of Cys to Ala).

Expression and purification of recombinant PrP (rPrP)

The expression plasmids based on pRSETB and pET22b(+) were introduced into *E. coli* BL21(DE3)*LysS* and JM109(DE3), respectively. Protein expression was induced by adding isopropylthio-β-D-galactoside to a final concentration at 0.4 mM. Two to four hours after induction, bacterial cells were collected and inclusion bodies were prepared as described elsewhere (Sambrook et al., 1989). The inclusion bodies from BL21(DE3)*LysS* transformed with pRSETB-based expression plasmids were solubilized with 6 M GdnHCl in 20 mM phosphate buffer (pH 7.8). The rPrP was further purified by Ni^{2+}-immobilized metal affinity chromatography (IMAC) using Ni^{2+}-charged Chelating Sepharose Fast flow (Amersham Pharmacia) and a

stepwise elution gradient from pH 4.9 to 4.3 in the presence of 6 M GdnHCl. Inclusion bodies from JM109(DE3) transformed with pET22b(+)-based expression plasmids were solubilized with 8 M Urea and 20 mM Tris–HCl, pH 8.0. Next, the urea concentration was reduced to 6 M, and the mixture was applied to DEAE-Sepharose equilibrated with 6 M Urea and 20 mM Tris–HCl, pH 8.0. The unbound fraction was saved for further purification. The rPrP in the eluate from IMAC and the unbound fraction from DEAE-Sepharose were dialyzed against 10 mM acetate buffer (ranging from pH 4.4 to 3.6). After the dialysis, rPrP containing an intramolecular disulfide bond was purified by reverse-phase HPLC using TSKgel Phenyl-5PW RP (TOSOH) and a 30–50% linear gradient of acetonitrile with 0.05% trifluoroacetic acid. The purified rPrP was lyophilized and dissolved with Mili-Q water at 1 mg/ml and stored at −20 °C.

Purification of PrP^{Sc} and formation of detergent-lipid-protein complexes (DLPC)

A mouse-adapted scrapie Obihiro strain (Shinagawa et al., 1985) was used in this study. ICR/Slc female mice were inoculated intracerebrally with 20 μl of brain homogenate of Obihiro strain infected-mice and were sacrificed under anesthesia when they showed the clinical symptoms of the terminal stage of the disease. PrP^{Sc} was purified from the scrapie-affected mice brains without proteinase K treatment as described by Bolton et al. (1987) with minor modifications (Caughey et al., 1991). Protein concentration was determined by DC protein assay kit (Bio-Rad).

Ten micrograms of purified PrP^{Sc} was suspended in 1.6 ml of DLPC buffer containing 2% Sarkosyl, 0.4% phosphatidylcholine, 150 mM NaCl, and 50 mM Tris–HCl, pH 8.3. The suspension was sonicated for five cycles of 2 s with a Branson Sonifier Contamination-free Ultrasonic Sample Pre-processing System.

Production of monoclonal antibodies

Purified PrP^{Sc}, rMoPrP23–231, or rMoPrP89–231 was mixed with an equal volume of Freund's complete adjuvant and 200 μg of each PrP was inoculated subcutaneously into PrP gene-ablated mice (Yokoyama et al., 2001). After the first immunization, the mice received 100 μg of the same PrP preparation with Freund's incomplete adjuvant twice every 2 weeks. The booster shot was given intraperitoneally with 50 μg of each PrP preparation in PBS. Three days after the booster, splenocytes obtained from immunized mice were fused with P3U1 mouse myeloma cells using polyethylene glycol 1500 (Roche Diagnostic) according to the supplier's instruction, and hybridomas were selected in HAT medium. Hybridoma culture supernatants were screened by ELISA using purified PrP^{Sc} and rMoPrP as described below. The hybridomas secreting mAbs were cloned by limiting dilution. The isotypes of the mAbs were determined using the IsoStrip mouse monoclonal antibody isotyping kit (Roche Diagnostic). Large-scale preparations of mAbs were carried out in INTEGRA CELLine high density culture units (IBS Integra Biosciences). The supernatants harvested from the units were concentrated by precipitation with 50% saturated ammonium sulfate and then purified by size exclusion chromatography with Superdex-200 HR (Amersham Pharmacia Biotech).

ELISA

Ninety-six well plates (MaxiSorp, Nunc) were coated overnight at 4 °C with either 200 ng/well of purified PrP^{Sc} or 100 ng/well of rMoPrP in 50 μl of 20 mM phosphate buffer, pH 7.0. After adsorption, wells were blocked with 5% fetal bovine serum (FBS) in PBS containing 0.1% Tween 20 (PBST) for 2 h at room temperature (r.t.), and then incubated with culture supernatants or antibodies diluted with 1% FBS in PBST for 1 h. After washing with PBST, wells were incubated with 100 μl of 1:2500 diluted HRP-conjugated $F(ab')_2$ fragment anti-mouse Ig (Amersham Bioscience) for 1 h. Finally, antigen–antibody complexes were detected by adding a substrate solution of 100 μg/ml of 2,2′-azino-bis(3-ethyl-benzthiazoline-6-sulfonic acid), 0.04% H_2O_2 in 50 mM citrate-phosphate buffer, pH 4.0, and the absorbance at 405 nm was measured with a microplate reader (Multiscan MS-UV, Labsystems). A ready to use 3,3′,5,5′-tetramethylbenzidine (TMB) was also used as a substrate, and the absorbance at 450 nm was measured for TMB.

Immunoblotting

The preparation of PrP^{Sc} and immunoblotting were carried out as described elsewhere (Grathwohl et al., 1997). The blots were developed with ECL Western blotting detection reagents (Amersham Pharmacia) and immunoreactive proteins were detected with X-ray film.

Pepspots analysis

In these studies, we used pepspots membrane to which an array of 99 overlapping synthetic peptides, corresponding to residues 23–231 of mouse PrP, was covalently attached to a cellulose support via carboxyl termini. Each peptide is 13 amino acid residues long, and there is a two amino acid shift along the mouse PrP amino acid sequence from one peptide to the next. The membrane was blocked with 5% skim milk and 5% sucrose in PBST, and then incubated with culture supernatants of hybridomas as primary antibodies. Bound antibodies were detected using a 1:2500 diluted HRP-conjugated $F(ab')_2$ fragment anti-mouse Ig and an ECL Western blotting detection reagent.

Acknowledgments

This work was supported by a grant from The 21st Century COE Program (A-1), and a Grant-in-Aid for Science Research (A) (grant 15208029) and (B) (grant 12460130) from the Ministry of Education, Culture, Sports, Science, and Technology, Japan. This work was also supported by a grant from the Ministry of Health, Labour and Welfare of Japan.

References

Barry, R.A., Prusiner, S.B., 1986. Monoclonal antibodies to the cellular and scrapie prion proteins. J. Infect. Dis. 154, 518–521.

Bolton, D.C., Bendheim, P.E., Marmorstein, A.D., Potempska, A., 1987. Isolation and structural studies of the intact scrapie agent protein. Arch. Biochem. Biophys. 258, 579–590.

Caughey, B.W., Dong, A., Bhat, K.S., Ernst, D., Hayes, S.F., Caughey, W.S., 1991. Secondary structure analysis of the scrapie-associated protein PrP 27–30 in water by infrared spectroscopy. Biochemistry 30, 7672–7680.

Caughey, B., Kocisko, D.A., Raymond, G.J., Lansbury Jr., P.T., 1995. Aggregates of scrapie-associated prion protein induce the cell-free conversion of protease-sensitive prion protein to the protease-resistant state. Chem. Biol. 2, 807–817.

Caughey, B., Raymond, G.J., Kocisko, D.A., Lansbury Jr., P.T., 1997. Scrapie infectivity correlates with converting activity, protease resistance, and aggregation of scrapie-associated prion protein in guanidine denaturation studies. J. Virol. 71, 4107–4110.

Gabizon, R., McKinley, M.P., Prusiner, S.B., 1987. Purified prion proteins and scrapie infectivity copartition into liposomes. Proc. Natl. Acad. Sci. U.S.A. 84, 4017–4021.

Gasset, M., Baldwin, M.A., Lloyd, D.H., Gabriel, J.M., Holtzman, D.M., Cohen, F., Fletterick, R., Prusiner, S.B., 1992. Predicted alpha-helical regions of the prion protein when synthesized as peptides form amyloid. Proc. Natl. Acad. Sci. U.S.A. 89, 10940–10944.

Grathwohl, K.U., Horiuchi, M., Ishiguro, N., Shinagawa, M., 1997. Sensitive enzyme-linked immunosorbent assay for detection of PrP(Sc) in crude tissue extracts from scrapie-affected mice. J. Virol. Methods 64, 205–216.

Harmeyer, S., Pfaff, E., Groschup, M.H., 1998. Synthetic peptide vaccines yield monoclonal antibodies to cellular and pathological prion proteins of ruminants. J. Gen. Virol. 79, 937–945.

Holscher, C., Delius, H., Burkle, A., 1998. Overexpression of nonconvertible PrPc delta114–121 in scrapie-infected mouse neuroblastoma cells leads to trans-dominant inhibition of wild-type PrP(Sc) accumulation. J. Virol. 72, 1153–1159.

Hope, J., Morton, L.J., Farquhar, C.F., Multhaup, G., Beyreuther, K., Kimberlin, R.H., 1986. The major polypeptide of scrapie-associated fibrils (SAF) has the same size, charge distribution and N-terminal protein sequence as predicted for the normal brain protein (PrP). EMBO J. 5, 2591–2597.

Horiuchi, M., Yamazaki, N., Ikeda, T., Ishiguro, N., Shinagawa, M., 1995. A cellular form of prion protein (PrPC) exists in many non-neuronal tissues of sheep. J. Gen. Virol. 76, 2583–2587.

Kaneko, K., Zulianello, L., Scott, M., Cooper, C.M., Wallace, A.C., James, T.L., Cohen, F.E., Prusiner, S.B., 1997. Evidence for protein X binding to a discontinuous epitope on the cellular prion protein during scrapie prion propagation. Proc. Natl. Acad. Sci. U.S.A. 94, 10069–10074.

Kanyo, Z.F., Pan, K.M., Williamson, R.A., Burton, D.R., Prusiner, S.B., Fletterick, R.J., Cohen, F.E., 1999. Antibody binding defines a structure for an epitope that participates in the PrPC → PrPSc conformational change. J. Mol. Biol. 293, 855–863.

Kascsak, R.J., Rubenstein, R., Merz, P.A., Tonna-DeMasi, M., Fersko, R., Carp, R.I., Wisniewski, H.M., Diringer, H., 1987. Mouse polyclonal and monoclonal antibody to scrapie-associated fibril proteins. J. Virol. 61, 3688–3693.

Korth, C., Stierli, B., Streit, P., Moser, M., Schaller, O., Fischer, R., Schulz-Schaeffer, W., Kretzschmar, H., Raeber, A., Braun, U., Ehrensperger, F., Hornemann, S., Glockshuber, R., Riek, R., Billeter, M., Wuthrich, K., Oesch, B., 1997. Prion (PrPSc)-specific epitope defined by a monoclonal antibody. Nature 390, 74–77.

Krasemann, S., Groschup, M.H., Harmeyer, S., Hunsmann, G., Bodemer, W., 1996. Generation of monoclonal antibodies against human prion proteins in PrP0/0 mice. Mol. Med. 2, 725–734.

Meyer, R.K., McKinley, M.P., Bowman, K.A., Braunfeld, M.B., Barry, R.A., Prusiner, S.B., 1986. Separation and properties of cellular and scrapie prion proteins. Proc. Natl. Acad. Sci. U.S.A. 83, 2310–2314.

Muramoto, T., Scott, M., Cohen, F.E., Prusiner, S.B., 1996. Recombinant scrapie-like prion protein of 106 amino acids is soluble. Proc. Natl. Acad. Sci. U.S.A. 93, 15457–15462.

O'Rourke, K.I., Baszler, T.V., Miller, J.M., Spraker, T.R., Sadler-Riggleman, I., Knowles, D.P., 1998. Monoclonal antibody F89/160.1.5 defines a conserved epitope on the ruminant prion protein. J. Clin. Microbiol. 36, 1750–1755.

Pan, K.M., Baldwin, M., Nguyen, J., Gasset, M., Serban, A., Groth, D., Mehlhorn, I., Huang, Z., Fletterick, R.J., Cohen, F.E., 1993. Conversion of alpha-helices into beta-sheets features in the formation of the scrapie prion proteins. Proc. Natl. Acad. Sci. U.S.A. 90, 10962–10966.

Paramithiotis, E., Pinard, M., Lawton, T., LaBoissiere, S., Leathers, V.L., Zou, W.Q., Estey, L.A., Lamontagne, J., Lehto, M.T., Kondejewski, L.H., Francoeur, G.P., Papadopoulos, M., Haghighat, A., Spatz, S.J., Head, M., Will, R., Ironside, J., O'Rourke, K., Tonelli, Q., Ledebur, H.C., Chakrabartty, A., Cashman, N.R., 2003. A prion protein epitope selective for the pathologically misfolded conformation. Nat. Med. 9, 893–899.

Peretz, D., Williamson, R.A., Matsunaga, Y., Serban, H., Pinilla, C., Bastidas, R.B., Rozenshteyn, R., James, T.L., Houghten, R.A., Cohen, F.E., Prusiner, S.B., Burton, D.R., 1997. A conformational transition at the N terminus of the prion protein features in formation of the scrapie isoform. J. Mol. Biol. 273, 614–622.

Prusiner, S.B., 1991. Molecular biology of prion diseases. Science 252, 1515–1522.

Prusiner, S.B., Groth, D., Serban, A., Stahl, N., Gabizon, R., 1993. Attempts to restore scrapie prion infectivity after exposure to protein denaturants. Proc. Natl. Acad. Sci. U.S.A. 90, 2793–2797.

Riek, R., Hornemann, S., Wider, G., Billeter, M., Glockshuber, R., Wuthrich, K., 1996. NMR structure of the mouse prion protein domain PrP(121–321). Nature 382, 180–182.

Safar, J., Roller, P.P., Gajdusek, D.C., Gibbs Jr., C.J., 1993. Conformational transitions, dissociation, and unfolding of scrapie amyloid (prion) protein. J. Biol. Chem. 268, 20276–20284.

Sambrook, J., Fritsch, E.F., Maniatis, T., 1989. Molecular Cloning: A Laboratory Manual. Cold Spring Harbor Press, Cold Spring Harbor, NY.

Serban, D., Taraboulos, A., DeArmond, S.J., Prusiner, S.B., 1990. Rapid detection of Creutzfeldt–Jakob disease and scrapie prion proteins. Neurology 40, 110–117.

Shinagawa, M., Takahashi, K., Sasaki, S., Doi, S., Goto, H., Sato, G., 1985. Characterization of scrapie agent isolated from sheep in Japan. Microbiol. Immunol. 29, 543–551.

Wille, H., Michelitsch, M.D., Guenebaut, V., Supattapone, S., Serban, A., Cohen, F.E., Agard, D.A., Prusiner, S.B., 2002. Structural studies of the scrapie prion protein by electron crystallography. Proc. Natl. Acad. Sci. U.S.A. 99, 3563–3568.

Williamson, R.A., Peretz, D., Smorodinsky, N., Bastidas, R., Serban, H., Mehlhorn, I., DeArmond, S.J., Prusiner, S.B., Burton, D.R., 1996. Circumventing tolerance to generate autologous monoclonal antibodies to the prion protein. Proc. Natl. Acad. Sci. U.S.A. 93, 7279–7282.

Williamson, R.A., Peretz, D., Pinilla, C., Ball, H., Bastidas, R.B., Rozenshteyn, R., Houghten, R.A., Prusiner, S.B., Burton, D.R., 1998. Mapping the prion protein using recombinant antibodies. J. Virol. 72, 9413–9418.

Wopfner, F., Weidenhofer, G., Schneider, R., von Brunn, A., Gilch, S.,